

MDM-Prime-v2: Binary Encoding and Index Shuffling Enable Compute-optimal Scaling of Diffusion Language Models

Chen-Hao Chao¹ Wei-Fang Sun² Junwei Quan¹ Chun-Yi Lee³ Rahul G. Krishnan¹

Abstract

Masked diffusion models (MDM) exhibit superior generalization when learned using a Partial masking scheme (Prime). This approach converts tokens into sub-tokens and models the diffusion process at the sub-token level. We identify two limitations of the MDM-Prime framework. First, we lack tools to guide the hyperparameter choice of the token granularity in the subtokenizer. Second, we find that the function form of the subtokenizer significantly degrades likelihood estimation when paired with commonly used Byte-Pair-Encoding (BPE) tokenizers. To address these limitations, we study the tightness of the variational bound in MDM-Prime and develop MDM-Prime-v2, a masked diffusion language model which incorporates *Binary Encoding* and *Index Shuffling*. Our scaling analysis reveals that MDM-Prime-v2 is $21.8\times$ more compute-efficient than autoregressive models (ARM). In compute-optimal comparisons, MDM-Prime-v2 achieves 7.77 perplexity on OpenWebText, outperforming ARM (12.99), MDM (18.94), and MDM-Prime (13.41). When extending the model size to 1.1B parameters, our model further demonstrates superior zero-shot accuracy on various commonsense reasoning tasks.

1. Introduction

Likelihood-based pretraining serves as the cornerstone of scalable language modeling (Kaplan et al., 2020; Hoffmann et al., 2022). Autoregressive models (ARM) (e.g., (Radford et al., 2019; Touvron et al., 2023)) and masked diffusion models (MDM) (e.g., (Sahoo et al., 2024; Nie et al., 2025b)) represent two paradigms: the former utilizes the chain rule to decompose the joint likelihood of the data, while the latter employs stochastic unmasking to reconstruct data from masked sequences. Currently, ARMs dominate

¹University of Toronto, Vector Institute ²NVIDIA AI Technology Center ³National Taiwan University. Correspondence to: Rahul G. Krishnan <rahulgk@cs.toronto.edu>.

Preprint. March 18, 2026.

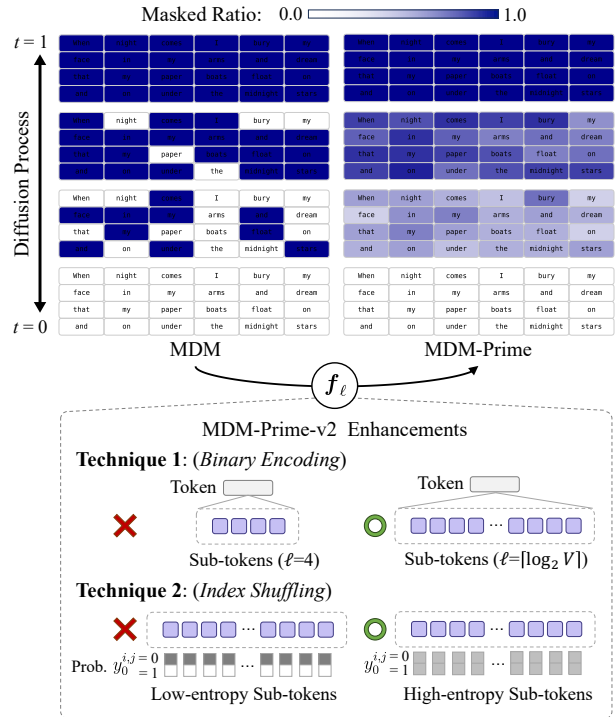


Figure 1. Overview of MDM, MDM-Prime, and the MDM-Prime-v2 enhancements. ℓ is the token granularity in base- b encoding and V is the vocabulary size. $y_0^{i,j}$ is a sub-token with positional indices i and j . MDM-Prime-v2 incorporates two techniques: Technique 1 sets $\ell = \lceil \log_2 V \rceil$ for f_ℓ , which performs binary encoding. Technique 2 employs an index shuffling operation to encode high-entropy sub-tokens. The gray cell intensity in the lower section represents sub-token probability when $y_0^{i,j} = 0$ or 1.

frontier language models, largely because they achieve more compute-efficient likelihood estimation when floating point operations (FLOPs) expand. In contrast, MDMs exhibit a $\sim 16\times$ efficiency deficit (Nie et al., 2025a); however, the root cause of this discrepancy remains underexplored.

Chao et al. (2025) showed that improving the expressivity of the latent representation of MDMs results in substantial improvement to perplexity and introduced a generalized class of MDM called MDM-Prime. This work reveals insights into effectively modeling likelihood with MDMs and offers a pathway toward mitigating the efficiency gap between ARMs and MDMs.

In MDMs, each token takes one of two states, *masked* or *unmasked*. MDM-Prime introduces a richer set of intermediate latent representations via partially masked tokens. MDM-Prime uses a subtokenizer f_ℓ with adjustable token granularity ℓ to encode each token into a sequence of ℓ sub-tokens. By modeling the diffusion process at the sub-token level, partially masked tokens can be produced naturally as intermediate transition states, leading to a finegrained denoising process, as illustrated in the upper section of Fig. 1.

However, MDM-Prime lacks a theoretical rationale for the performance improvements stemming from its subtokenizer design, leaving the underlying relationship between the subtokenizer and the model’s likelihood estimation capability unexplored. We investigate two fundamental questions regarding f_ℓ . First, instead of treating ℓ as an empirically tuned hyperparameter, we derive an explicit relationship between ℓ and the tightness of the variational bound, establishing a principled criterion for its selection. Second, we identify a link between the subtokenizer, which determines how the model perceives inputs, and the tokenizer, which defines the data distribution. Our analysis of f_ℓ reveals that high-entropy sub-tokens tighten the variational bound. Based on this insight, we introduce a technique called index shuffling to permute token indices. We integrate these improvements into a unified framework named MDM-Prime-v2.

We perform a scaling analysis of MDM-Prime v2 against ARMs and MDMs. By varying compute budgets from 3×10^{18} to 3×10^{20} FLOPs, we determine compute-optimal configurations for all three model types. We find that MDM-Prime-v2 achieves an evaluation perplexity of 7.77 on OpenWebText (Gokaslan et al., 2019), outperforming the compute-optimal baselines of ARM (12.99), MDM (18.94), and MDM-Prime (13.41). We scale MDM-Prime-v2 to 1.1B parameters and our model demonstrates superior performance over similar-sized baselines including GPT-Neo (Black et al., 2021), OPT (Zhang et al., 2022), Pythia (Biderman et al., 2023), Bloom (BigScience, 2023), SMDM (Nie et al., 2025a) and TinyLLaMA (Zhang et al., 2024) on zero-shot commonsense reasoning benchmarks. The contributions of this work are summarized as follows:

- We examine the variational bound of MDM-Prime and characterize how token granularity and sub-token distributions influence the tightness of the bound.
- Based on the aforementioned analysis, we establish two practical techniques: a selection criterion for ℓ under which f_ℓ performs binary encoding, and a technique to enhance sub-token entropy, called index shuffling.
- We demonstrate that MDM-Prime-v2 outperforms compute-optimal ARMs across various compute budgets. At the 1.1B parameter scale, it achieves state-of-the-art zero-shot commonsense reasoning performance.

2. Background

2.1. Masked Diffusion Models

Let $\mathbf{x} = [x^1, \dots, x^L] \in \mathcal{X}^L$ be a sequence of L tokens¹, where x^i denotes an element of \mathbf{x} and $\mathcal{X} \triangleq \{0, \dots, V-1\}$ represents a set of V token indices. Given a continuous time variable $t \in [0, 1]$, $\mathbf{x}_0 \in \mathcal{X}^L$ denote the sample drawn from the data distribution q_{data} , and $\mathbf{x}_t \in (\mathcal{X} \cup \{\text{m}\})^L \triangleq \tilde{\mathcal{X}}^L$ denotes the latent variable introduced by the forward diffusion process, where *m* represents the masked token. Let $\delta_{x'}(x)$ be the Kronecker delta function, which equals 1 if $x = x'$ and 0 otherwise. The forward diffusion process is performed through a kernel $q_\alpha(\mathbf{x}_t | \mathbf{x}_0) = \prod_{i=1}^L q_\alpha(x_t^i | x_0^i)$ following a strictly decreasing time-dependent scheduling function $\alpha_t : [0, 1] \rightarrow [0, 1]$. The element-wise kernel q_α is defined as follows (Sahoo et al., 2024; Shi et al., 2024):

$$q_\alpha(x_t^i | x_0^i) = (1 - \alpha_t)\delta_{\text{m}}(x_t^i) + \alpha_t\delta_{x_0^i}(x_t^i). \quad (1)$$

The negative log-likelihood (NLL) of the data distribution $\mathbb{E}_{q_{\text{data}}(\mathbf{x}_0)}[-\log p(\mathbf{x}_0)]$ can be approximated using a variational upper bound, expressed as follows (Sahoo et al., 2024; Shi et al., 2024; Xu et al., 2025; Zheng et al., 2025):

$$\mathcal{L}_{\text{vb}} = \int_0^1 \frac{\alpha'_t}{1 - \alpha_t} \mathbb{E}_{q_\alpha(\mathbf{x}_0, \mathbf{x}_t)} [\log p(\mathbf{x}_0 | \mathbf{x}_t)] dt, \quad (2)$$

where $\alpha'_t = \frac{d}{dt}\alpha_t$ and $q(\mathbf{x}_0, \mathbf{x}_t) \triangleq q_{\text{data}}(\mathbf{x}_0)q_\alpha(\mathbf{x}_t | \mathbf{x}_0)$. $p(\mathbf{x}_0 | \mathbf{x}_t)$ is a parametric function, satisfying the *carry-over* condition (Sahoo et al., 2024) (i.e., the marginal $p(x_0^i | \mathbf{x}_t) = \delta_{x_t^i}(x_0^i)$ for position i where $x_t^i \in \mathcal{X}$ is unmasked (Chao et al., 2025)) and typically factorized as $\prod_{i=1}^L p(x_0^i | \mathbf{x}_t)$.

Let $s, t \in [0, 1]$ be time variables such that $s < t$. The reverse diffusion process is performed by iteratively applying $p(\mathbf{x}_s | \mathbf{x}_t) = \mathbb{E}_{p(\mathbf{x}_0 | \mathbf{x}_t)} [q_\alpha(\mathbf{x}_s | \mathbf{x}_t, \mathbf{x}_0)]$ (Austin et al., 2021), by first drawing $\mathbf{x}_0 \sim p(\cdot | \mathbf{x}_t)$ and then sampling $\mathbf{x}_s \sim q_\alpha(\cdot | \mathbf{x}_t, \mathbf{x}_0)$ in each timestep, starting from $t = 1$. The reverse kernel $q_\alpha(\mathbf{x}_s | \mathbf{x}_t, \mathbf{x}_0) = \prod_{i=1}^L q_\alpha(x_s^i | x_t^i, x_0^i)$ is defined as:

$$q_\alpha(x_s^i | x_t^i, x_0^i) = \begin{cases} \delta_{x_t^i}(x_s^i), & \text{if } x_t^i \in \mathcal{X}, \\ \frac{1 - \alpha_s}{1 - \alpha_t} \delta_{\text{m}}(x_s^i) + \frac{\alpha_s - \alpha_t}{1 - \alpha_t} \delta_{x_0^i}(x_s^i), & \text{if } x_t^i = \text{m}. \end{cases} \quad (3)$$

Intuitively, each masked token transitions to its original value x_0^i with probability $\frac{\alpha_s - \alpha_t}{1 - \alpha_t}$ and retains the masked value with probability $\frac{1 - \alpha_s}{1 - \alpha_t}$.

2.2. Generalization via Partial Masking

Given the token granularity ℓ , MDM-Prime (Chao et al., 2025) represents each token $x_0^i \in \mathcal{X}$ as a sequence

¹Text is mapped to discrete random variables (tokens) via Byte-Pair Encoding (BPE) tokenizer, following the standard practice of GPT (Radford et al., 2019) and LLaMA (Touvron et al., 2023).

of ℓ sub-tokens $\mathbf{y}_0^i = [y_0^{i,1}, \dots, y_0^{i,\ell}] \in \mathcal{Y}^\ell$ via an invertible function $f_\ell : \mathcal{X} \rightarrow \mathcal{Y}^\ell$, known as subtokenizer, where $\mathcal{Y} \triangleq \{0, \dots, b-1\}$ denotes a set of sub-token indices with $b = \lceil \sqrt[\ell]{V} \rceil \in \mathbb{N}$. The vectorized function f_ℓ applied to the full sequence is defined as: $\mathbf{f}_\ell(\mathbf{x}_0) \triangleq [f_\ell(x_0^1), \dots, f_\ell(x_0^L)] = [\mathbf{y}_0^1, \dots, \mathbf{y}_0^L] = [(y_0^{1,1}, \dots, y_0^{1,\ell}), \dots, (y_0^{L,1}, \dots, y_0^{L,\ell})] = \mathbf{y}_0$. The maximum ℓ for f_ℓ is $\lceil \log_2 V \rceil$, where the function encodes tokens into binary sub-tokens. This operation is composable: for granularities ℓ_1, ℓ_2 such that $\frac{\ell_2}{\ell_1} \in \mathbb{N}$, the transformation can be decomposed as $\mathbf{f}_{\ell_2} = \mathbf{f}_{\ell_2/\ell_1} \circ \mathbf{f}_{\ell_1}$. MDM-Prime employs standard base- b encoding for f_ℓ , denoted as $\mathbf{f}_\ell \triangleq \mathbf{f}_{\text{base-}b}$, and implements it using a lookup table.

The latent variable $\mathbf{y}_t \in (\mathcal{Y} \cup \{m\})^{L \times \ell} \triangleq \tilde{\mathcal{Y}}^{L \times \ell}$ is sampled through independent masking, analogous to Eq. (1). The forward diffusion kernel $q_\alpha(\mathbf{y}_t | \mathbf{y}_0) = \prod_{i=1}^L \prod_{j=1}^\ell q_\alpha(y_t^{i,j} | y_0^{i,j})$ is defined as follows:

$$q_\alpha(y_t^{i,j} | y_0^{i,j}) = (1 - \alpha_t) \delta_m(y_t^{i,j}) + \alpha_t \delta_{y_0^{i,j}}(y_t^{i,j}). \quad (4)$$

Since f_ℓ is invertible and both \mathbf{x}_0 and \mathbf{y}_0 are discrete, the change-of-variable principle indicates that the NLL is invariant: $\mathbb{E}_{q_{\text{data}}(\mathbf{x}_0)}[-\log p(\mathbf{x}_0)] = \mathbb{E}_{q_{\text{data},\mathbf{y}}(\mathbf{y}_0)}[-\log p_\ell(\mathbf{y}_0)]$, where $q_{\text{data},\mathbf{y}}(\mathbf{y}_0) \triangleq q_{\text{data}} \circ \mathbf{f}_\ell^{-1}(\mathbf{y}_0)$ and $p_\ell(\mathbf{y}_0)$ represent the modeled distributions. Therefore, MDM-Prime approximates the same objective as MDM by substituting \mathbf{x}_0 as \mathbf{y}_0 . The variational bound can be expressed in a similar way as Eq. (2):

$$\mathcal{L}_{\text{vb}}^{(\ell)} = \int_0^1 \frac{\alpha'_t}{1 - \alpha_t} \mathbb{E}_{q_\alpha(\mathbf{y}_0, \mathbf{y}_t)} [\log p_\ell(\mathbf{y}_0 | \mathbf{y}_t)] dt, \quad (5)$$

where $q_\alpha(\mathbf{y}_0, \mathbf{y}_t) = q_{\text{data},\mathbf{y}}(\mathbf{y}_0) q_\alpha(\mathbf{y}_t | \mathbf{y}_0)$, and $p_\ell(\mathbf{y}_0 | \mathbf{y}_t)$ denotes the MDM-Prime model.

Adapting the model architecture from MDM to MDM-Prime requires only a simple modification of the embedding lookup table. In this setup, sub-token embeddings are aggregated into token embeddings and subsequently processed by the neural network at the token level. This design preserves the computational cost (FLOPs) of each training iteration. A detailed description of the model architecture is provided in Appendix A.2.1 and Fig. A2 (a).

3. Methodology

This section details two proposed enhancements: Section 3.1 discusses the token granularity selection and Section 3.2 explores improved function form for the subtokenizer.

3.1. Tightening Variational Bound via Binary Encoding

The value of ℓ is critical to the performance of MDM-Prime. However, its specific influence on the loss function and the criteria for a reliable selection have not been well explored.

In this section, we propose setting ℓ to its maximum viable value, $\ell = \lceil \log_2 V \rceil$. To justify this choice, we first establish in **Proposition 3.1** that the variational bound of MDM-Prime is monotonically non-increasing with respect to ℓ . We then describe the conditions under which the bound becomes strictly tighter in **Proposition 3.2**. Detailed proofs are provided in Appendix A.1.1.

Proposition 3.1. *Let p and p_ℓ denote the MDM and MDM-Prime models. Let ℓ_1, ℓ_2 be token granularities satisfying $1 < \ell_1 < \ell_2$ and $\frac{\ell_2}{\ell_1} \in \mathbb{N}$. The following inequalities hold:*

$$\inf_p \mathcal{L}_{\text{vb}} \geq \inf_{p_{\ell_1}} \mathcal{L}_{\text{vb}}^{(\ell_1)} \geq \inf_{p_{\ell_2}} \mathcal{L}_{\text{vb}}^{(\ell_2)}. \quad (6)$$

While Eq. (6) indicates that the loss optimum is non-increasing with respect to ℓ , it remains inconclusive regarding selection when the equalities hold. We address this by characterizing the equality conditions in **Proposition 3.2**.

Proposition 3.2. *Let $\tilde{\ell} \in \mathbb{N}$ and $\mathbf{g}_{\tilde{\ell}}$ be a vectorized mapping with element-wise operation defined as:*

$$\mathbf{g}_{\tilde{\ell}}(\mathbf{y}_t^i) = \begin{cases} f_{\tilde{\ell}}^{-1}(\mathbf{y}_t^i), & \text{if } y_t^{i,j} \neq m, \forall j \in \{1, \dots, \tilde{\ell}\}, \\ m, & \text{otherwise,} \end{cases} \quad (7)$$

Given a scheduling function α_t and defining $\tilde{\alpha}_t = \alpha_t^{1/\tilde{\ell}}$, the first inequality in Eq. (6) becomes an equality if and only if:

$$\mathbb{E}_{q_{\tilde{\alpha}}(\mathbf{y}_t)} \left[\mathbb{D}_{\text{KL}}(q_{\text{data},\mathbf{y}}(\mathbf{y}_0 | \mathbf{y}_t) \| q_{\text{data},\mathbf{y}}(\mathbf{y}_0 | \mathbf{g}_{\tilde{\ell}}(\mathbf{y}_t))) \right] = 0, \quad (8)$$

where $\mathbf{y}_0 \in \mathcal{Y}^{L \times \ell_1}$, $\mathbf{y}_t \in \tilde{\mathcal{Y}}^{L \times \ell_1}$, $\tilde{\ell} = \ell_1$, and the second inequality becomes an equality if and only if Eq. (8) holds with $\tilde{\ell} = \frac{\ell_2}{\ell_1}$, $\mathbf{y}_0 \in \mathcal{Y}^{L \times \ell_2}$, and $\mathbf{y}_t \in \tilde{\mathcal{Y}}^{L \times \ell_2}$.

The equality condition Eq. (8) requires the KL divergence to be zero, implying the two conditional distributions must be identical. However, the two distributions differ in their conditioning variables: the first distribution uses \mathbf{y}_t , while the second is conditioned on $\mathbf{g}_{\tilde{\ell}}(\mathbf{y}_t)$. As defined in Eq. (7), $\mathbf{g}_{\tilde{\ell}}$ maps a sequence of sub-tokens \mathbf{y}_t^i to the corresponding token $f_{\tilde{\ell}}^{-1}(\mathbf{y}_t^i)$ when no masked sub-token is present; otherwise, it returns the masked token m . Replacing sub-tokens with a mask discards information and alters the predictive distribution of \mathbf{y}_0 . Consequently, the equality can hold only in the degenerate case where each sub-token carries no information about \mathbf{y}_0 .

Based on **Propositions 3.1** and **3.2**, increasing ℓ yields a tighter variational bound. Based on this finding, we propose the following selection principle for the token granularity:

Technique 1. (Binary Encoding) Select $\ell = \lceil \log_2 V \rceil$ such that \mathbf{f}_ℓ encodes tokens into binary sub-tokens.

3.2. Increasing Sub-token Entropy via Index Shuffling

While Section 3.1 identifies the optimal value of ℓ for a given invertible subtokenizer \mathbf{f}_ℓ , the form of \mathbf{f}_ℓ remains an open

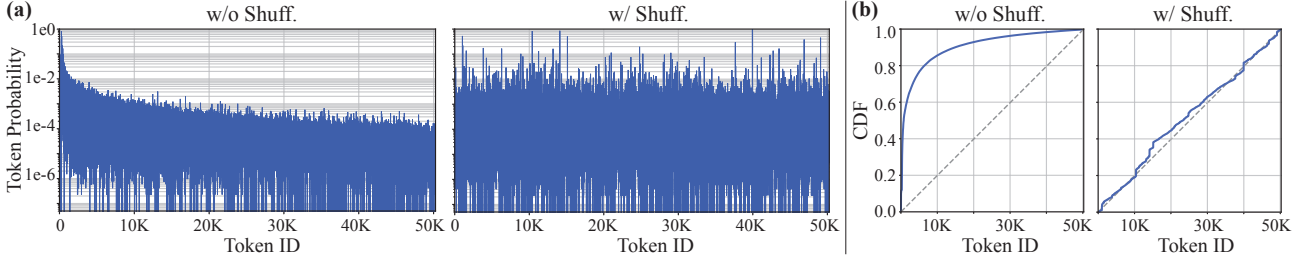


Figure 2. (a) Token probability and (b) cumulative distribution function (CDF) over token indices of the GPT-2 tokenizer (Radford et al., 2019) evaluated on the C4 dataset (Raffel et al., 2020). The left and right subplots of (a) and (b) show setups without and with index shuffling, respectively. The gray dashed line in (b) represents the CDF of a uniform token distribution.

question. Instead of defining $f_\ell \triangleq f_{\text{base-}b}$, this section derives the condition for f_ℓ to minimize the variational bound. Let f_{shuffle} denote an *Index Shuffling* operation, which permutes token indices via a lookup table (see Appendix A.2.2 and Fig. A2 (b)). We propose $f_\ell \triangleq f_{\text{base-}b} \circ f_{\text{shuffle}}$, which integrates f_{shuffle} to effectively approximate the optimum.

To pinpoint the effect of f_ℓ on the objective (Eq. (5)), we isolate the term in the variational bound that depend on the transformation. We present this decomposition in **Proposition 3.3** (proof in Appendix A.1.2).

Proposition 3.3. *The variational bound can be decomposed into f_ℓ -independent and -dependent terms as follows:*

$$\inf_{f_\ell} \inf_{p_\ell} \mathcal{L}_{vb}^{(\ell)} = \int_0^1 \frac{\alpha'_t}{1 - \alpha_t} \left(\underbrace{-\mathcal{H}(\mathbf{y}_0, \mathbf{y}_t)}_{\text{Independent on } f_\ell} + \sup_{f_\ell} \underbrace{\mathcal{H}(\mathbf{y}_t)}_{\text{Dependent on } f_\ell} \right) dt, \quad (9)$$

where $\mathcal{H}(\mathbf{y}_t) \triangleq \mathbb{E}_{q_\alpha(\mathbf{y}_t)}[-\log q_\alpha(\mathbf{y}_t)]$ and $\mathcal{H}(\mathbf{y}_0, \mathbf{y}_t) \triangleq \mathbb{E}_{q_\alpha(\mathbf{y}_0, \mathbf{y}_t)}[-\log q_\alpha(\mathbf{y}_0, \mathbf{y}_t)]$ represent the entropy of \mathbf{y}_t and the joint entropy of $\mathbf{y}_0, \mathbf{y}_t$, respectively.

The f_ℓ -independent term corresponds to the joint negative entropy $-\mathcal{H}(\mathbf{y}_0, \mathbf{y}_t) = -(\mathcal{H}(\mathbf{y}_0) + \mathcal{H}(\mathbf{y}_t|\mathbf{y}_0))$, where $\mathcal{H}(\mathbf{y}_0) = \mathcal{H}(\mathbf{x}_0)$ remains constant due to the invertibility of f_ℓ , while $\mathcal{H}(\mathbf{y}_t|\mathbf{y}_0)$ is determined solely by the forward kernel in Eq. (4). On the other hand, the f_ℓ -dependent term suggests that the optimal f_ℓ should maximize the entropy of \mathbf{y}_t , which reaches its optimum when each unmasked $y_t^{i,j}$ is uniformly distributed on \mathcal{Y} , as shown in **Proposition 3.4**:

Proposition 3.4. *The entropy of \mathbf{y}_t is bounded:*

$$\mathcal{H}(\mathbf{y}_t) \leq L\ell(h(\alpha_t) + \alpha_t \log b), \quad (10)$$

where $h(\alpha_t) \triangleq -(1 - \alpha_t) \log(1 - \alpha_t) - \alpha_t \log \alpha_t$. The equality holds if and only if each unmasked $y_t^{i,j}$ is uniformly distributed on \mathcal{Y} .

Although **Propositions 3.3** and **3.4** identify high-entropy sub-tokens as the ideal case for optimality, the sub-tokens generated by directly applying base- b encoding to the token indices from commonly-used BPE tokenizers exhibit low

Table 1. Entropy of sub-tokens across different ℓ . The results are evaluated on C4 (Raffel et al., 2020). The maximum entropy is given by $-\log_2 \frac{1}{b}$, where $b = \lceil \sqrt[\ell]{V} \rceil$ and $V = 50,257$. $\lceil \log_2 V \rceil = 16$ represents the maximum of ℓ . Three configurations are compared: (1) ‘w/o Shuff.’, the baseline setup without index shuffling, (2) ‘w/ Shuff. (25%)’, the setup where the shuffling operation is applied only to the first 25% of the token indices, and (3) ‘w/ Shuff.’, the setup where token indices are fully shuffled.

	w/o Shuff.	w/ Shuff. (25%)	w/ Shuff.	Maximum
$\ell = 16$	0.8146	0.9038	0.9936	1.0000
$\ell = 8$	1.6152	1.8040	1.9811	2.0000
$\ell = 4$	3.2051	3.5360	3.8553	3.9069
$\ell = 2$	6.1489	6.7880	7.2803	7.8138

entropy. An example of the GPT-2 tokenizer (Radford et al., 2019) is presented in the ‘w/o Shuff.’ column of Table 1. This occurs since BPE is constructed by iteratively merging the most frequent subword pairs. As a result, token probability is inversely proportional to the token index (see the left subplots with title ‘w/o Shuff.’ in Fig. 2 (a) and (b)). Directly encoding these structured token indices using base- b encoding results in sub-tokens with low entropy, contradicting the maximization goal in Eqs. (9) and (10). To effectively disrupt the inherent token index structure, we propose the following technique:

Technique 2. (Index Shuffling) Randomly shuffle the token indices before performing base- b encoding.

An illustrative example is provided in Fig. 3 (a) to demonstrate how randomly shuffled token indices lead to higher sub-token entropy. By applying Technique 2, the average entropy approaches the theoretical maximum ($-\log_2 \frac{1}{b}$), as demonstrated in the ‘w/ Shuff.’ and ‘w/ Shuff. (25%)’ columns of Table 1. Furthermore, as illustrated in Fig. 4, the NLL decreases significantly when augmented with this shuffling operation. Unlike the standard configuration (i.e., ‘w/o Shuff.’) where the loss plateaus or even slightly increases after $\ell = 4$, the loss of the shuffled setup decreases monotonically and outperforms the compute-optimal ARM by a noticeable margin, confirming the empirical effectiveness of this technique. The significant reduction in loss stems from increased certainty in the conditional (predictive) distribution $q_{\text{data-}y}(\mathbf{y}_0|\mathbf{y}_t)$. As depicted in Fig. 3 (b), the

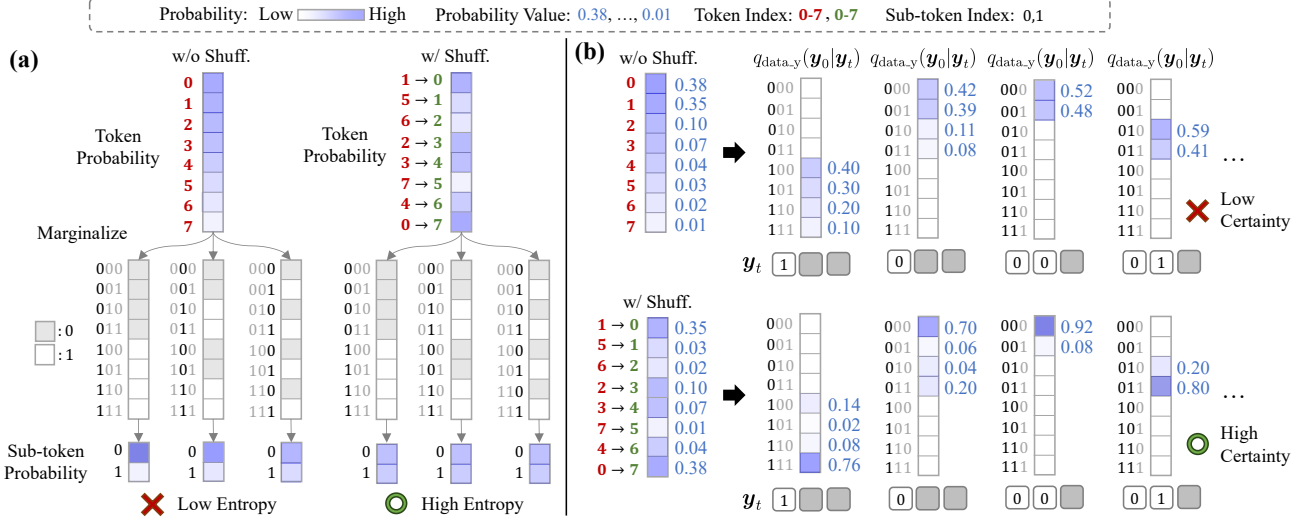


Figure 3. Illustrative examples of the index shuffling operation proposed in Technique 2. In this plot, $V = 8$, $\ell = 3$ and $b = 2$. Color intensity represents probability values, where darker blue denotes higher probability. (a) Marginal distributions: Marginalization is performed by summing entries corresponding to sub-token indices 0 (gray) and 1 (white), respectively. Sub-tokens encoded from standard token indices (i.e., ‘w/o Shuff.’) exhibit low entropy, while the shuffling operation results in sub-tokens with higher entropy. A detailed numerical example are provided in Fig. A3 in Appendix. (b) Conditional (predictive) distribution: The distribution $q_{\text{data},y}(\mathbf{y}_0|\mathbf{y}_t)$ exhibits higher certainty under index shuffling, which results in improved likelihood estimation.

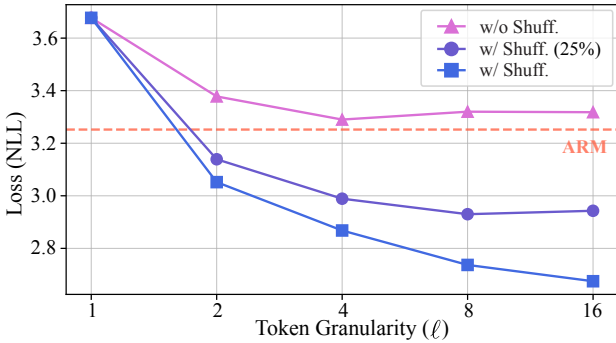


Figure 4. The NLL of MDM ($\ell = 1$) and MDM-Prime ($\ell > 1$) under three setups: ‘w/o Shuff.’, ‘w/ Shuff. (25%)’, and ‘w/ Shuff.’ [$\log_2 V = 16$ represents the maximum of ℓ]. The red dashed line represent the NLL of the compute-optimal ARM. All models are trained using 10^{19} FLOPs. The experiments are conducted on C4.

index shuffling operation scatters similar probability masses across different slots. Therefore, when a specific sub-token value is observed, the conditional distribution becomes more certain, leading to improved likelihood estimation.

In summary, Techniques 1 and 2 suggest the following sub-tokenizer: $f_\ell = f_{\text{base-}b} \circ f_{\text{shuffle}}$, where $f_{\text{base-}b}$ performs binary encoding with $\ell = \lceil \log_2 V \rceil$, while f_{shuffle} maps the original token indices into shuffled ones. The entire operation is implemented using lookup tables, requiring zero FLOPs and can be performed during data preprocessing. Further specifications are available in Appendix A.2.2 and Fig. A2 (b).

4. Experiments

This section evaluates MDM-Prime-v2 via scaling analysis (Section 4.1), the OpenWebText benchmark (Section 4.2),

Table 2. The coefficients (\hat{a} and \hat{b}) derived using the Chinchilla scaling law. A larger \hat{a} indicates that compute resources should prioritize model parameters, while a larger \hat{b} indicates that compute resources should prioritize training tokens. The other coefficients (α , β , A , B , and E) are provided in Table A3 in Appendix.

Coefficient	$\hat{a} (N_{\text{opt}} \propto C^{\hat{a}})$	$\hat{b} (D_{\text{opt}} \propto C^{\hat{b}})$
ARM	0.45	0.55
MDM	0.43	0.57
MDM-Prime-v2 ($\ell=16$)	0.42	0.58

and 1.1B-scale pretraining (Section 4.3). Training details are provided in Appendix A.3. In Appendix A.4, we validate f_{shuffle} ’s robustness to random seed initialization, demonstrate MDM-Prime-v2’s improved sample quality, and discuss the ineffectiveness of subtokenization for ARMs. We also provide insights into MDM-Prime-v2’s performance gains by analyzing its attention patterns and the long-tailed singular value spectra of its projection weights.

4.1. Loss Behavior and Scaling Properties

As established in (Kaplan et al., 2020; Hoffmann et al., 2022), the NLL of language models exhibits a strong correlation with the training FLOPs (C). This compute budget is primarily determined by two configuration factors: the total number of training tokens (D) and the number of non-embedding parameters (N). To understand how they influence the likelihood modeling ability of the proposed method, we analyze ARM, MDM, and MDM-Prime-v2 across various combinations of N and D under fixed compute budgets ranging from 3×10^{18} to 3×10^{20} FLOPs. For these experiments, we employ a Transformer (Vaswani et al.,

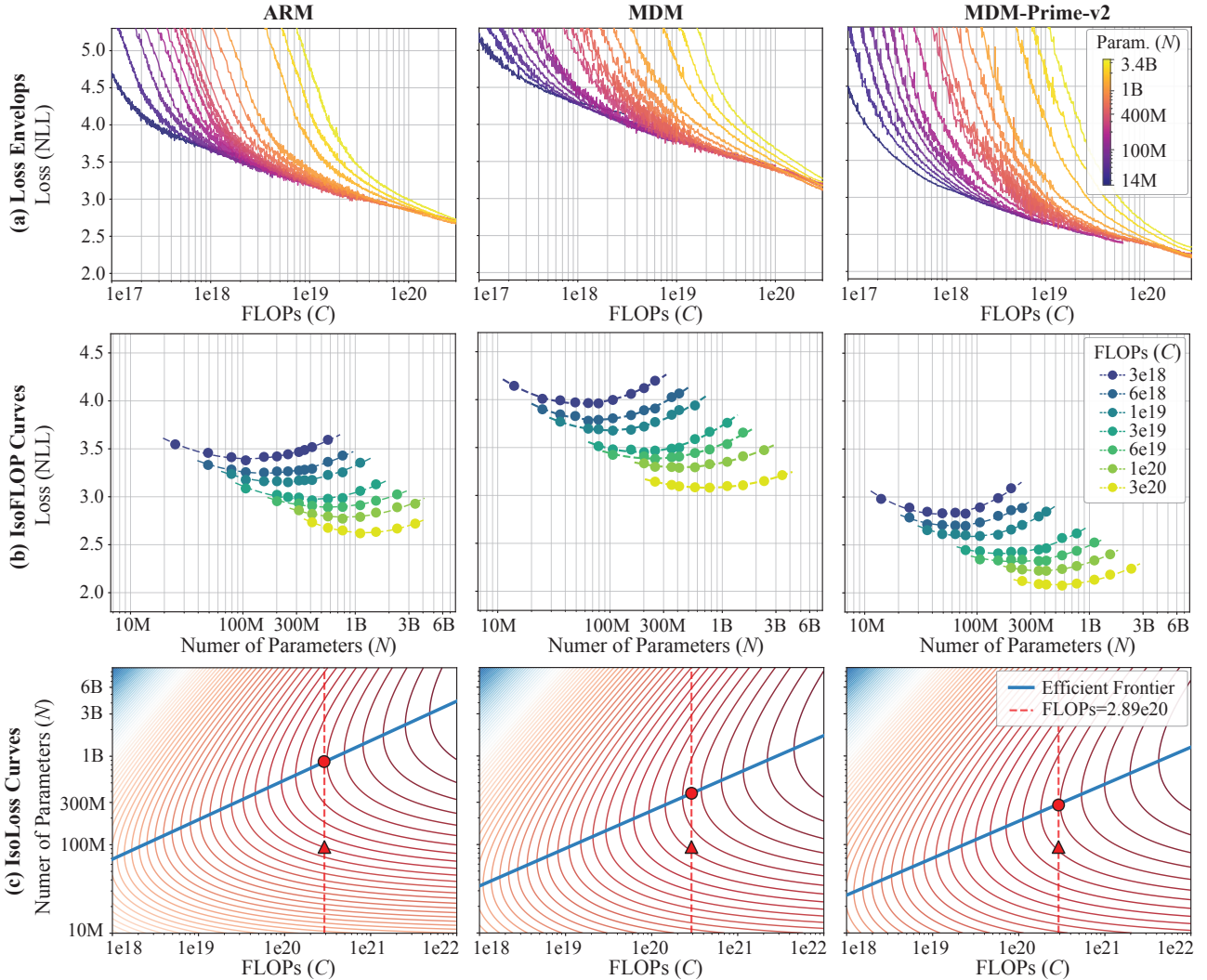


Figure 5. The (a) loss envelopes, (b) isoFLOP curves, and (c) isoloss curves of ARM, MDM, and MDM-Prime-v2. In subplots (a), the number of parameters (N) ranges from 14M (purple) to 3.4B (yellow). In subplots (b), the compute budget (C) ranges from 3×10^{18} FLOPs (blue) to 3×10^{20} FLOPs (yellow). In subplots (c), the curves represent loss contours, the solid blue line denotes the efficient frontier, and the red dashed line represents the 2.89×10^{20} FLOPs setup adopted in Section 4.2. Triangular markers represent the configuration used by (Sahoo et al., 2024), while circular markers denote the compute-optimal setup.

2017) architecture incorporating RoPE (Su et al., 2023), SwiGLU (Shazeer, 2020), and QK-normalization (Dehghani et al., 2023). All models are trained on C4 (Raffel et al., 2020) using the GPT-2 tokenizer with $V = 50, 257$.

Figs. 5 (a), (b), and (c) present the loss envelopes, isoFLOP, and isoloss curves for ARM, MDM, and MDM-Prime-v2. As shown in Fig. 5 (a), the training loss for all three methods decreases consistently as the total compute budget increases. This confirms that their likelihood modeling capabilities scale effectively with training FLOPs. Fig. 5 (b) compares model performance across fixed compute budgets. By analyzing the minima of the isoFLOP contours, we observe that MDM-Prime-v2 consistently achieves a lower compute-optimal loss than both ARM and MDM. These results verify that MDM-Prime-v2 is the most compute-efficient among

the three methods across all tested scales. According our further analysis in Appendix A.4.5, MDM-Prime-v2 is $21.8\times$ more compute-efficient than ARMs. Finally, we employ the Chinchilla scaling law (Hoffmann et al., 2022) to analyze loss behavior. Using our empirical observations, consisting of (loss, N , D) triplets, we fit the power-law loss estimator: $\hat{\mathcal{L}}(N, D) = E + \frac{A}{N^\alpha} + \frac{B}{D^\beta}$, where α, β, A, B , and E are coefficients determined via regression. Under a fixed compute budget $C \approx 6ND$, the optimal allocation of parameters (N_{opt}) and tokens (D_{opt}) is derived as follows:

$$N_{\text{opt}} = G \left(\frac{C}{6} \right)^{\hat{a}}, \quad D_{\text{opt}} = G^{-1} \left(\frac{C}{6} \right)^{\hat{b}}, \quad (11)$$

where $G = \left(\frac{\alpha A}{\beta B} \right)^{\frac{1}{\alpha+\beta}}$, $\hat{a} = \frac{\beta}{\alpha+\beta}$, and $\hat{b} = \frac{\alpha}{\alpha+\beta}$. As shown

Table 3. PPL evaluation on OWT. Methods marked with * are trained with a compute-optimal setup, where the non-embedding parameters (N) and number of training tokens (D) are optimized based on the efficient frontier line presented in Fig. 5 (c). The total compute is fixed at 2.89×10^{20} FLOPs for all models. The compute-optimal setup for MDM-Prime is approximated using that of MDM-Prime-v2. The symbol \downarrow represents that lower values correspond to better performance. MDM in this table represents MDLM (Sahoo et al., 2024).

	N	D	PPL (\downarrow)
Order-Specific Models			
BD3-LMs (Arriola et al., 2025)	92M	524B	≤ 20.73
EDLM-coAR (Xu et al., 2025)	92M	524B	≤ 17.58
ARM (Sahoo et al., 2024)	92M	524B	17.54
Order-Agnostic Models			
Duo (Sahoo et al., 2025)	92M	524B	≤ 25.20
SEDD (Lou et al., 2024)	92M	524B	≤ 24.10
MDM (Sahoo et al., 2024)	92M	524B	≤ 22.98
GenMD4 (Shi et al., 2024)	92M	524B	≤ 21.80
EDLM-NCE (Xu et al., 2025)	92M	524B	≤ 21.52
MDM-Prime ($\ell=2$) (Chao et al., 2025)	92M	524B	≤ 17.90
MDM-Prime ($\ell=4$) (Chao et al., 2025)	92M	524B	≤ 15.62
MDM-Prime ($\ell=6$) (Chao et al., 2025)	92M	524B	≤ 15.36
MDM-Prime ($\ell=8$) (Chao et al., 2025)	92M	524B	≤ 15.48
MDM-Prime-v2 ($\ell=16$) (Ours)	92M	524B	≤ 8.47
ARM*	860M	56B	12.99
MDM*	375M	128B	≤ 18.94
MDM-Prime* ($\ell=6$)	286M	168B	≤ 13.41
MDM-Prime-v2* ($\ell=16$) (Ours)	286M	168B	≤ 7.77

in Table 2, ARM exhibits the largest \hat{a} and the smallest \hat{b} , indicating that the compute-optimal configuration of ARM prioritizes increasing model capacity (N) over data volume (D). In contrast, MDM-Prime-v2 yields the smallest \hat{a} and the largest \hat{b} , suggesting that its compute-optimal performance is driven more by increasing training tokens than by expanding model parameters. These coefficients determine the compute-optimal frontier lines (i.e., the blue straight lines) illustrated in Fig. 5 (c). The ARM frontier is shifted toward larger models (upward/left), whereas the MDM-Prime-v2 frontier is shifted toward longer training (downward/right). These results serve as a diagnostic tool for compute efficiency. For example, a commonly-used training configuration in MDM research (Sahoo et al., 2024) adopts $N=92\text{M}$, $D=524\text{B}$, which falls short of the compute-optimal frontier for all three models (as indicated by the gap between \blacktriangle and \bullet in Fig. 5 (c)). To understand how this discrepancy affects model ranking, the following section offers a further analysis on the OpenWebText (OWT) benchmark.

4.2. Improvement to Likelihood Evaluation

In this experiment, we follow (Sahoo et al., 2024) to train models on the OWT dataset (Gokaslan et al., 2019). We

compare performance using perplexity (PPL) (i.e., exponential of NLL) on a held-out OWT validation set and across six zero-shot textual benchmarks. The dataset is tokenized using the GPT-2 tokenizer with a vocabulary size of $V = 50,257$. Following the prior work (Sahoo et al., 2024), all of the models employ the same architecture based on a diffusion transformer (DiT) (Peebles & Xie, 2022) with RoPE (Su et al., 2023). Appendix A.3.2 provides details regarding the configuration of the model architecture. The results are presented in Tables 3 and 4.

We observe that performance is sensitive to the allocation of N and D under a fixed compute budget. As demonstrated in Table 3, ARM’s PPL improves significantly, from 17.54 to 12.99 (i.e., the difference between ARM and ARM* is 4.55), simply by adjusting these two parameters. In addition, the baseline configuration ($N=92\text{M}$, $D=524\text{B}$), which uses excessively large D , appears to inadvertently favor the MDM-based approaches, evidenced by the relatively small gains observed in MDM, MDM-Prime, and MDM-Prime-v2 when shifting to the compute-optimal setup. This observation also consolidates our findings in Section 4.1, which suggest that MDM-based methods scale more effectively when trained on an abundance of tokens (i.e., larger \hat{b}).

By calibrating all models to the compute-optimal setup (denoted with *), we establish a consistent and fair criterion for performance evaluation. Under this configuration, MDM-Prime-v2* outperforms ARM*, MDM-Prime*, and MDM* by noticeable margins of 5.22, 5.64, and 11.17 PPL, respectively. These results verify the effectiveness of our two proposed techniques in enhancing model performance.

To assess generalizability across diverse textual domains, we evaluate the models on a suite of zero-shot benchmarks, including LAMBADA (Paperno et al., 2016), WikiText (Merity et al., 2016), PTB (Marcus et al., 1993), LM1B (Chelba et al., 2013), AG News (Zhang et al., 2015), and ArXiv (Cohan et al., 2018). As shown in Table 4, MDM-Prime-v2* consistently achieves superior results across all benchmarks, highlighting its generalizability across multiple domains.

4.3. Improvement to Larger-Scale Pretraining

In this experiment, we adopt the training configuration of TinyLLaMA (ARM) (Zhang et al., 2024) and SMDM (MDM) (Nie et al., 2025a) to train a 1.1B parameter model on 540B tokens from the Slimpajama dataset (Soboleva et al., 2023) (totaling 3.3×10^{21} FLOPs). As discussed in Appendix A.3.3, this setup is compute-optimal for MDM and near-optimal for both ARM and MDM-Prime-v2. We compare the models on a wide-range commonsense reasoning tasks, including SciQ (Welbl et al., 2017), SocialQA (Sap et al., 2019), McTaco (Zhou et al., 2019), TruthfulQA (Lin et al., 2022), BoolQ (Clark et al., 2019a), ANLI (Nie et al., 2020), ARC-e (easy) (Clark et al., 2018),

Table 4. Zero-shot validation perplexities evaluated on six textual datasets. Lower values correspond to better performance. All models are trained on OWT with their training perplexity shown in Table 3. MDM in this table represents MDLM (Sahoo et al., 2024).

	LAMBADA (\downarrow)	WikiText (\downarrow)	PTB (\downarrow)	LM1B (\downarrow)	AG News (\downarrow)	ArXiv (\downarrow)
ARM (Sahoo et al., 2024)	51.28	25.75	82.05	51.25	52.09	41.73
BD3-LM (Arriola et al., 2025)	≤ 50.03	≤ 31.31	≤ 96.81	≤ 60.88	≤ 61.67	≤ 39.20
EDLM-coAR (Xu et al., 2025)	≤ 50.04	≤ 28.31	≤ 89.73	≤ 60.23	≤ 57.94	≤ 39.02
Duo (Sahoo et al., 2025)	≤ 49.78	≤ 33.57	≤ 89.35	≤ 73.86	≤ 67.81	≤ 40.39
SEDD (Lou et al., 2024)	≤ 49.86	≤ 34.28	≤ 100.09	≤ 68.20	≤ 62.09	≤ 38.48
EDLM-NCE (Xu et al., 2025)	≤ 46.92	≤ 30.77	≤ 93.21	≤ 63.19	≤ 60.02	≤ 36.63
MDM (Sahoo et al., 2024)	≤ 47.52	≤ 32.83	≤ 95.26	≤ 67.01	≤ 61.15	≤ 37.37
MDM-Prime ($\ell=2$) (Chao et al., 2025)	≤ 30.91	≤ 27.93	≤ 74.81	≤ 55.50	≤ 63.21	≤ 25.44
MDM-Prime ($\ell=4$) (Chao et al., 2025)	≤ 24.44	≤ 23.86	≤ 53.98	≤ 38.02	≤ 59.44	≤ 25.83
MDM-Prime ($\ell=6$) (Chao et al., 2025)	≤ 25.80	≤ 26.87	≤ 62.62	≤ 45.36	≤ 60.16	≤ 25.19
MDM-Prime ($\ell=8$) (Chao et al., 2025)	≤ 25.23	≤ 25.77	≤ 53.77	≤ 38.00	≤ 64.89	≤ 25.79
MDM-Prime-v2 ($\ell=16$) (Ours)	≤ 28.40	≤ 26.05	≤ 24.50	≤ 20.23	≤ 33.72	≤ 31.28
ARM*	37.52	22.28	103.25	43.20	39.35	29.82
MDM*	≤ 40.43	≤ 26.65	≤ 87.29	≤ 60.96	≤ 51.44	≤ 31.89
MDM-Prime* ($\ell=6$)	≤ 36.15	≤ 19.46	≤ 44.49	≤ 41.28	≤ 48.09	≤ 26.24
MDM-Prime-v2* ($\ell=16$) (Ours)	≤ 12.37	≤ 12.51	≤ 20.26	≤ 16.57	≤ 27.79	≤ 18.22

Table 5. Zero-shot accuracies evaluated on eight commonsense reasoning benchmarks. Higher values correspond to better performance.

	SciQ	SocialQA	McTaco	TruthfulQA	BoolQ	ANLI	ARC-e	OBQA	Avg.
GPT-Neo (1.3B) (Black et al., 2021)	77.10	41.25	42.89	23.13	61.99	33.13	50.21	33.60	45.41
OPT (1.3B) (Zhang et al., 2022)	76.70	40.63	37.08	23.75	57.83	33.86	50.97	33.40	44.28
Pythia (1.4B) (Biderman et al., 2023)	79.20	40.94	54.25	22.77	63.15	33.29	53.91	33.20	47.59
Bloom (1.1B) (BigScience, 2023)	74.60	39.05	53.63	25.58	59.08	33.35	45.41	29.40	45.01
SMDM (1.1B) (Nie et al., 2025a)	81.20	41.04	35.07	24.60	62.17	32.81	48.74	33.40	44.88
TinyLLaMA (1.1B) (Zhang et al., 2024)	80.90	39.56	40.88	20.93	59.20	33.25	52.40	33.40	45.07
MDM-Prime-v2 (1.1B) (Ours)	83.30	42.02	66.14	25.83	62.05	34.24	47.81	34.00	49.42

and OBQA (Mihaylov et al., 2018). The descriptions of these tasks are available in Table A5 in Appendix. The model architecture and tokenizer are based on LLaMA (Touvron et al., 2023), and the vocabulary size is $V = 32,000$.

Table 5 presents the results. We compare our method against several pretrained ARM and MDM baselines of similar size: GPT-Neo (1.3B), OPT (1.3B), Pythia (1.4B), Bloom (1.1B), SMDM (1.1B), and TinyLLaMA (1.1B). MDM-Prime-v2 achieves the highest average accuracy across the tasks, outperforming these baselines on six of the eight tasks. In particular, our model demonstrates advantages in temporal reasoning and scientific question answering, delivering significant gains on the McTaco and SciQ benchmarks.

5. Related Works

The foundational framework for discrete diffusion was established by (Sohl-Dickstein et al., 2015) and subsequently expanded to real-world generative tasks via D3PM (Austin et al., 2021) and CTMC (Campbell et al., 2022). Recent efforts have adapted these principles to large language modeling, where MDMs (Sahoo et al., 2024; Shi et al., 2024) have emerged as a particularly scalable framework among various discrete diffusion alternatives (Gulrajani & Hashimoto, 2023; Gat et al., 2024). While the scaling behav-

ior of MDMs have been thoroughly investigated under both compute-constrained (Nie et al., 2025a; Ni et al., 2025; von Rütte et al., 2025) and data-constrained (Prabhudesai et al., 2025) regimes, a significant efficiency gap remains: Nie et al. (2025a) demonstrated that standard MDMs are $16\times$ less efficient than ARMs in compute-optimal setups. We bridge this gap by identifying the impact of the subtokenizer on the scaling behavior of MDMs. Through a comprehensive evaluation, we demonstrate that MDM-Prime-v2 is, to the best of our knowledge, the first order-agnostic framework to achieve superior compute-optimality compared to ARMs. As shown in Fig. A9 in Appendix, MDM-Prime-v2 is approximately $21.8\times$ more compute-efficient than ARM.

6. Conclusion

We present MDM-Prime-v2, an enhanced version of the MDM-Prime model. Our analysis identifies a critical connection between the token granularity ℓ and the variational bound, revealing the sub-optimality of base- b encoding for f_ℓ with BPE tokenizers. We resolve these issues by selecting $\ell = \lceil \log_2 V \rceil$ and employing an index shuffling operation in the subtokenizer design. We characterize the scaling behavior of MDM-Prime-v2, showing consistent improvements across varying model and data scales. These

gains translate to practical performance, as evidenced by our 1.1B parameter model, which achieves improvements on zero-shot reasoning benchmarks.

Impact Statement

We investigate the theoretical properties of MDM-Prime and introduce MDM-Prime-v2 as an effective practical instantiation. As our work aims to advance the fundamentals of Machine Learning, we do not identify specific negative societal consequences that must be highlighted here.

References

- Ainslie, J., Lee-Thorp, J., de Jong, M., Zemlyanskiy, Y., Lebrón, F., and Sanghai, S. GQA: Training Generalized Multi-Query Transformer Models from Multi-Head Checkpoints. In *Proc. Conf. Empirical Methods in Natural Language Processing (EMNLP)*, 2023.
- Arriola, M., Gokaslan, A., Chiu, J. T., Yang, Z., Qi, Z., Han, J., Sahoo, S. S., and Kuleshov, V. Block Diffusion: Interpolating Between Autoregressive and Diffusion Language Models. In *Proc. Int. Conf. on Learning Representations (ICLR)*, 2025.
- Austin, J., Johnson, D. D., Ho, J., Tarlow, D., and van den Berg, R. Structured Denoising Diffusion Models in Discrete State-Spaces. In *Proc. of the Int. Conf. on Neural Information Processing Systems (NeurIPS)*, 2021.
- Biderman, S., Schoelkopf, H., Anthony, Q. G., Bradley, H., O’Brien, K., Hallahan, E., Khan, M. A., Purohit, S., Prashanth, U. S., Raff, E., et al. Pythia: A suite for analyzing large language models across training and scaling. In *Proc. Int. Conf. on Machine Learning (ICML)*, 2023.
- BigScience. BLOOM: A 176B-Parameter Open-Access Multilingual Language Model, 2023.
- Black, S., Gao, L., Wang, P., Leahy, C., and Biderman, S. GPT-Neo: Large Scale Autoregressive Language Modeling with Mesh-Tensorflow, 2021.
- Campbell, A., Benton, J., Bortoli, V. D., Rainforth, T., Deligiannidis, G., and Doucet, A. A Continuous Time Framework for Discrete Denoising Models. In *Proc. of Int. Conf. on Neural Information Processing Systems (NeurIPS)*, 2022.
- Chao, C.-H., Sun, W.-F., Liang, H., Lee, C.-Y., and Krishnan, R. G. Beyond Masked and Unmasked: Discrete Diffusion Models via Partial Masking. In *Proceedings of the Conference on Neural Information Processing Systems (NeurIPS)*, 2025.
- Chelba, C., Mikolov, T., Schuster, M., Ge, Q., Brants, T., Koehn, P., and Robinson, T. One Billion Word Benchmark for Measuring Progress in Statistical Language Modeling. In *Proc. Conf. of the European Chapter of the Association for Computational Linguistics (EACL)*, 2013.
- Clark, C., Lee, K., Chang, M.-W., Kwiatkowski, T., Collins, M., and Toutanova, K. BoolQ: Exploring the Surprising Difficulty of Natural Yes/No Questions. In *Proc. Conf. of the North American Chapter of the Association for Computational Linguistics (NAACL)*, 2019a.
- Clark, K., Khandelwal, U., Levy, O., and Manning, C. D. What Does BERT Look At? An Analysis of BERT’s Attention. In *Proc. BlackboxNLP Workshop at Annual Meeting of the Association for Computational Linguistics (ACL)*, 2019b.
- Clark, P., Cowhey, I., Etzioni, O., Khot, T., Sabharwal, A., Schoenick, C., and Tafjord, O. Think you have Solved Question Answering? Try ARC, the AI2 Reasoning Challenge. 2018.
- Cohan, A., Dernoncourt, F., Kim, D. S., Bui, T., Kim, S., Chang, W., and Goharian, N. A Discourse-Aware Attention Model for Abstractive Summarization of Long Documents. In *Proc. Conf. of the North American Chapter of the Association for Computational Linguistics (NAACL)*, 2018.
- Dao, T., Fu, D. Y., Ermon, S., Rudra, A., and Ré, C. FlashAttention: Fast and Memory-Efficient Exact Attention with IO-Awareness. 2022.
- Dehghani, M., Djolonga, J., Mustafa, B., Padlewski, P., Heek, J., Gilmer, J., Steiner, A. P., Caron, M., Geirhos, R., Alabdulmohsin, I., Jenatton, R., Beyer, L., Tschannen, M., Arnab, A., Wang, X., Riquelme Ruiz, C., Minderer, M., Puigcerver, J., Evci, U., Kumar, M., Steenkiste, S. V., Elsayed, G. F., Mahendran, A., Yu, F., Oliver, A., Huot, F., Bastings, J., Collier, M., Gritsenko, A. A., Birodkar, V., Vasconcelos, C. N., Tay, Y., Mensink, T., Kolesnikov, A., Pavetic, F., Tran, D., Kipf, T., Lucic, M., Zhai, X., Keysers, D., Harmsen, J. J., and Houlsby, N. Scaling Vision Transformers to 22 Billion Parameters. In *Proc. Int. Conf. on Machine Learning (ICML)*, 2023.
- Dong, Y., Cordonnier, J.-B., and Loukas, A. Attention is Not All You Need: Pure Attention Loses Rank Doubly Exponentially with Depth. In *Proc. Int. Conf. on Machine Learning (ICML)*, 2021.
- Gao, L., Tow, J., Abbasi, B., Biderman, S., Black, S., DiPofi, A., Foster, C., Golding, L., Hsu, J., Le Noac’h, A., Li, H., McDonnell, K., Muennighoff, N., Ociepa, C., Phang, J., Reynolds, L., Schoelkopf, H., Skowron, A., Sutawika, L., Tang, E., Thite, A., Wang, B., Wang, K., and Zou, A. The Language Model Evaluation Harness. 2024.

- Gat, I., Remez, T., Shaul, N., Kreuk, F., Chen, R. T. Q., Synnaeve, G., Adi, Y., and Lipman, Y. Discrete Flow Matching. In *Proc. of Int. Conf. on Neural Information Processing Systems (NeurIPS)*, 2024.
- Gokaslan, A., Cohen, V., Pavlick, E., and Tellex, S. Open-webtext corpus. 2019.
- Gulrajani, I. and Hashimoto, T. B. Likelihood-Based Diffusion Language Models. In *Proc. of Int. Conf. on Neural Information Processing Systems (NeurIPS)*, 2023.
- Hoffmann, J., Borgeaud, S., Mensch, A., Buchatskaya, E., Cai, T., Rutherford, E., de Las Casas, D., Hendricks, L. A., Welbl, J., Clark, A., Hennigan, T., Noland, E., Millican, K., van den Driessche, G., Damoc, B., Guy, A., Osindero, S., Simonyan, K., Elsen, E., Rae, J. W., Vinyals, O., and Sifre, L. Training Compute-Optimal Large Language Models. In *Proc. of the Int. Conf. on Neural Information Processing Systems (NeurIPS)*, 2022.
- Kaplan, J., McCandlish, S., Henighan, T., Brown, T. B., Chess, B., Child, R., Gray, S., Radford, A., Wu, J., and Amodei, D. Scaling Laws for Neural Language Models. 2020.
- Kingma, D. P., Salimans, T., Poole, B., and Ho, J. Variational Diffusion Models. In *Proc. of the Int. Conf. on Neural Information Processing Systems (NeurIPS)*, 2021.
- Lefaudeux, B., Massa, F., Liskovich, D., Xiong, W., Caggiano, V., Naren, S., Xu, M., Hu, J., Tintore, M., Zhang, S., Labatut, P., Haziza, D., Wehrstedt, L., Reizenstein, J., and Sizov, G. xFormers: A modular and hackable Transformer modelling library. 2022.
- Lightning-AI. Lit-gpt. *arXiv preprint arXiv:1909.08053*, 2023.
- Lin, C.-Y. ROUGE: A Package for Automatic Evaluation of Summaries. In *Proc. Annual Meeting of the Association for Computational Linguistics (ACL)*, 2004.
- Lin, S., Hilton, J., and Evans, O. TruthfulQA: Measuring how models mimic human falsehoods. In *Proc. Association for Computational Linguistics (ACL)*, pp. 3214–3252, 2022. doi: 10.18653/v1/2022.acl-long.229.
- Loshchilov, I. and Hutter, F. Decoupled Weight Decay Regularization. In *Proc. Int. Conf. on Learning Representations (ICLR)*, 2019.
- Lou, A., Meng, C., and Ermon, S. Discrete Diffusion Modeling by Estimating the Ratios of the Data Distribution. In *Proc. Int. Conf. on Machine Learning (ICML)*, 2024.
- Marcus, M. P., Santorini, B., and Marcinkiewicz, M. A. Building a large annotated corpus of english: The penn treebank. *Computational Linguistics (CL)*, pp. 313–330, 1993.
- Martin, C. H. and Mahoney, M. W. Traditional and Heavy-Tailed Self Regularization in Neural Network Models, 2019.
- Merity, S., Xiong, C., Bradbury, J., and Socher, R. Pointer Sentinel Mixture Models. *arXiv:1609.07843 [cs.CL]*, 2016.
- Mihaylov, T., Clark, P., Khot, T., and Sabharwal, A. Can a Suit of Armor Conduct Electricity? A New Dataset for Open Book Question Answering, 2018.
- Ni, J., Liu, Q., Du, C., Dou, L., Yan, H., Wang, Z., Pang, T., and Shieh, M. Q. Training Optimal Large Diffusion Language Models. 2025.
- Nie, S., Zhu, F., Du, C., Pang, T., Liu, Q., Zeng, G., Lin, M., and Li, C. Scaling up masked diffusion models on text. In *Proc. Int. Conf. on Learning Representations (ICLR)*, 2025a.
- Nie, S., Zhu, F., You, Z., Zhang, X., Ou, J., Hu, J., Zhou, J., Lin, Y., Wen, J.-R., and Li, C. Large Language Diffusion Models. In *Proc. of Int. Conf. on Neural Information Processing Systems (NeurIPS)*, 2025b.
- Nie, Y., Williams, A., Dinan, E., Bansal, M., Weston, J., and Kiela, D. Adversarial NLI: A New Benchmark for Natural Language Understanding. In *Proc. Annual Meeting of the Association for Computational Linguistics (ACL)*, 2020.
- Paperno, D., Kruszewski, G., Lazaridou, A., Pham, N. Q., Bernardi, R., Pezzelle, S., Baroni, M., Boleda, G., and Fernández, R. The LAMBADA dataset: Word prediction requiring a broad discourse context. In *Proc. Annual Meeting of the Association for Computational Linguistics (ACL)*, 2016.
- Peebles, W. and Xie, S. Scalable Diffusion Models with Transformers. In *Int. Conf. Computer Vision (ICCV)*, 2022.
- Pillutla, K., Swayamdipta, S., Zellers, R., Thickstun, J., Welleck, S., Choi, Y., and Harchaoui, Z. MAUVE: Measuring the Gap Between Neural Text and Human Text using Divergence Frontiers. In *Proc. of Int. Conf. on Neural Information Processing Systems (NeurIPS)*, 2021.
- Prabhudesai, M., Wu, M., Zadeh, A., Fragkiadaki, K., and Pathak, D. Diffusion Beats Autoregressive in Data-Constrained Settings. In *Proc. of Int. Conf. on Neural Information Processing Systems (NeurIPS)*, 2025.
- Radford, A., Wu, J., Child, R., Luan, D., Amodei, D., and Sutskever, I. Language Models are Unsupervised Multi-task Learners. 2019.

- Raffel, C., Shazeer, N., Roberts, A., Lee, K., Narang, S., Matena, M., Zhou, Y., Li, W., and Liu, P. J. Exploring the Limits of Transfer Learning with a Unified Text-to-Text Transformer. *Journal of Machine Learning Research*, 21 (1), 2020. ISSN 1532-4435.
- Rashkin, H., Celikyilmaz, A., Choi, Y., and Gao, J. PlotMachines: Outline-Conditioned Generation with Dynamic Plot State Tracking. In *Proc. Conf. Empirical Methods in Natural Language Processing (EMNLP)*, 2020.
- Sahoo, S. S., Arriola, M., Schiff, Y., Gokaslan, A., Marroquin, E., Chiu, J. T., Rush, A., and Kuleshov, V. Simple and Effective Masked Diffusion Language Models. In *Proc. of the Int. Conf. on Neural Information Processing Systems (NeurIPS)*, 2024.
- Sahoo, S. S., Deschenaux, J., Gokaslan, A., Wang, G., Chiu, J., and Kuleshov, V. The Diffusion Duality. In *Proc. Int. Conf. on Machine Learning (ICML)*, 2025.
- Sap, M., Rashkin, H., Chen, D., Le Bras, R., and Choi, Y. Social IQa: Commonsense Reasoning about Social Interactions. In *Proc. Conf. Empirical Methods in Natural Language Processing (EMNLP)*, 2019.
- Shazeer, N. GLU Variants Improve Transformer. 2020.
- Shi, J., Han, K., Wang, Z., Doucet, A., and Titsias, M. K. Simplified and Generalized Masked Diffusion for Discrete Data. In *Proc. of the Int. Conf. on Neural Information Processing Systems (NeurIPS)*, 2024.
- Shoeybi, M., Patwary, M., Puri, R., LeGresley, P., Casper, J., and Catanzaro, B. Megatron-LM: Training Multi-Billion Parameter Language Models Using Model Parallelism. *arXiv preprint arXiv:1909.08053*, 2019.
- Soboleva, D., Al-Khateeb, F., Myers, R., Steeves, J. R., Hestness, J., and Dey, N. SlimPajama: A 627B token cleaned and deduplicated version of RedPajama, 2023.
- Sohl-Dickstein, J., Weiss, E. A., Maheswaranathan, N., and Ganguli, S. Deep Unsupervised Learning using Nonequilibrium Thermodynamics. In *Proc. Int. Conf. on Machine Learning (ICML)*, 2015.
- Su, J., Lu, Y., Pan, S., Murtadha, A., Wen, B., and Liu, Y. RoFormer: Enhanced Transformer with Rotary Position Embedding. 2023.
- Touvron, H., Lavril, T., Izacard, G., Martinet, X., Lachaux, M.-A., Lacroix, T., Rozière, B., Goyal, N., Hambro, E., Azhar, F., Rodriguez, A., Joulin, A., Grave, E., and Lample, G. LLaMA: Open and Efficient Foundation Language Models. *arXiv:2302.13971 [cs.CL]*, 2023.
- Vaswani, A., Shazeer, N., Parmar, N., Uszkoreit, J., Jones, L., Gomez, A. N., Kaiser, L., and Polosukhin, I. Attention Is All You Need. In *Proc. of the Int. Conf. on Neural Information Processing Systems (NeurIPS)*, 2017.
- von Rütte, D., Fluri, J., Pooladzandi, O., Schölkopf, B., Hofmann, T., and Orvieto, A. Scaling Behavior of Discrete Diffusion Language Models, 2025.
- Welbl, J., Liu, N. F., and Gardner, M. Crowdsourcing multiple choice science questions. In *Proc. Conf. Empirical Methods in Natural Language Processing (EMNLP)*, 2017.
- Xiao, G., Tian, Y., Chen, B., Han, S., and Lewis, M. Efficient Streaming Language Models with Attention Sinks. In *Proc. Int. Conf. on Learning Representations (ICLR)*, 2024.
- Xu, M., Geffner, T., Kreis, K., Nie, W., Xu, Y., Leskovec, J., Ermon, S., and Vahdat, A. Energy-Based Diffusion Language Models for Text Generation. In *Proc. Int. Conf. on Learning Representations (ICLR)*, 2025.
- Zhang, B. and Sennrich, R. Root Mean Square Layer Normalization. In *Proc. of the Int. Conf. on Neural Information Processing Systems (NeurIPS)*, 2019.
- Zhang, P., Zeng, G., Wang, T., and Lu, W. Tinyllama: An open-source small language model, 2024.
- Zhang, S., Roller, S., Goyal, N., Artetxe, M., Chen, M., Chen, S., Dewan, C., Diab, M., Li, X., Lin, X. V., Mihaylov, T., Ott, M., Shleifer, S., Shuster, K., Simig, D., Koura, P. S., Sridhar, A., Wang, T., and Zettlemoyer, L. OPT: Open Pre-trained Transformer Language Models, 2022.
- Zhang, X., Zhao, J., and LeCun, Y. Character-level Convolutional Networks for Text Classification. In *Proc. of Int. Conf. on Neural Information Processing Systems (NeurIPS)*, 2015.
- Zheng, K., Chen, Y., Mao, H., Liu, M.-Y., Zhu, J., and Zhang, Q. Masked Diffusion Models are Secretly Time-Agnostic Masked Models and Exploit Inaccurate Categorical Sampling. In *Proc. Int. Conf. on Learning Representations (ICLR)*, 2025.
- Zhong, M., Yin, D., Yu, T., Zaidi, A., Mutuma, M., Jha, R., Awadallah, A. H., Celikyilmaz, A., Liu, Y., Qiu, X., and Radev, D. QMSum: A New Benchmark for Query-based Multi-domain Meeting Summarization. In *Proc. Conf. of the North American Chapter of the Association for Computational Linguistics (NAACL)*, 2021.
- Zhou, B., Khashabi, D., Ning, Q., and Roth, D. "Going on a vacation" takes longer than "Going for a walk": A

Study of Temporal Commonsense Understanding. In *Proc. Conf. Empirical Methods in Natural Language Processing (EMNLP)*, 2019.

A. Appendix

In this appendix, we provide additional discussions and experiments. Section A.1 presents theoretical analyses. Section A.2 offers technical implementation details of the model architecture and subtokenizer of MDM-Prime-v2. Section A.3 elaborates on the experimental configurations. Section A.4 reports additional experimental results. Finally, Section A.5 outlines limitations and directions for future work.

A.1. Theoretical Analyses

In this section, we present theoretical derivations. In Section A.1.1, we present the proofs of **Propositions 3.1** and **3.2**, while Section A.1.2 establishes the justifications for **Propositions 3.3** and **3.4**. A table of symbols used in this paper is presented in Table A1.

Table A1. A table of symbols.

Symbol	Definition	Symbol	Definition
L	token sequence length	V	number of classes a token can take
ℓ	sub-token sequence length	b	number of classes a sub-token can take
\mathcal{X}	a set of tokens: $\{1, \dots, V-1\}$	$\tilde{\mathcal{X}}$	an augmented set of tokens: $\mathcal{X} \cup \{m\}$
\mathcal{Y}	a set of sub-tokens: $\{1, \dots, b-1\}$	$\tilde{\mathcal{Y}}$	an augmented set of sub-tokens: $\mathcal{Y} \cup \{m\}$
\mathbf{x}_0	a sequence of clean tokens ($\mathbf{x}_0 \in \mathcal{X}^L$)	\mathbf{x}_t	a sequence of noised tokens ($\mathbf{x}_t \in \tilde{\mathcal{X}}^L$)
\mathbf{y}_0	a sequence of clean sub-tokens ($\mathbf{y}_0 \in \mathcal{Y}^{L \times \ell}$)	\mathbf{y}_t	a sequence of noised sub-tokens ($\mathbf{y}_t \in \tilde{\mathcal{Y}}^{L \times \ell}$)
$\delta_x(x')$	Kronecker delta (equals 1 only if $x = x'$)	α_t	scheduling function ($\alpha_t : [0, 1] \rightarrow [0, 1]$)
$\mathbf{f}_\ell(\mathbf{x}_0)$	invertible base- b encoding	$\mathbf{g}_\ell(\mathbf{y}_t)$	a function that maps between latent variables
$p(\mathbf{x}_0 \mathbf{x}_t)$	MDM model (<i>carry-over</i> distribution of \mathbf{x}_0)	$p_\ell(\mathbf{y}_0 \mathbf{y}_t)$	MDM-Prime model (<i>carry-over</i> distribution of \mathbf{y}_0)
$q_{\text{data}}(\mathbf{x}_0)$	data distribution of \mathbf{x}_0	$q_{\text{data},\mathbf{y}}(\mathbf{y}_0)$	data distribution of \mathbf{y}_0 ($q_{\text{data},\mathbf{y}} = q_{\text{data}} \circ \mathbf{f}_\ell^{-1}$)

A.1.1. PROOF OF PROPOSITIONS 3.1 AND 3.2

We present our main findings (**Propositions 3.1** and **3.2**) as a merged **Theorem A.1**. The proof relies on a series of auxiliary results provided in **Lemmas A.2-A.4** and **Propositions A.5-A.6**.

Theorem A.1. *Let p and p_ℓ denote the MDM and MDM-Prime models. Let ℓ_1, ℓ_2 be token granularities satisfying $1 < \ell_1 < \ell_2$ and $\frac{\ell_2}{\ell_1} \in \mathbb{N}$. The following inequalities hold:*

$$\inf_p \mathcal{L}_{vb} \geq \inf_{p_{\ell_1}} \mathcal{L}_{vb}^{(\ell_1)} \geq \inf_{p_{\ell_2}} \mathcal{L}_{vb}^{(\ell_2)}. \quad (\text{A1})$$

Let $\tilde{\ell} \in \mathbb{N}$ and $\mathbf{g}_{\tilde{\ell}}$ be a vectorized mapping with element-wise operation defined as:

$$\mathbf{g}_{\tilde{\ell}}(\mathbf{y}_t^i) = \begin{cases} \mathbf{f}_{\tilde{\ell}}^{-1}(\mathbf{y}_t^i), & \text{if } y_t^{i,j} \neq m, \forall j \in \{1, \dots, \tilde{\ell}\}, \\ m, & \text{otherwise,} \end{cases} \quad (\text{A2})$$

Given a scheduling function α_t and defining $\tilde{\alpha}_t = \alpha_t^{1/\tilde{\ell}}$, the first inequality in Eq. (A1) becomes an equality if and only if:

$$\mathbb{E}_{q_{\tilde{\alpha}}(\mathbf{y}_t)} \left[\mathbb{D}_{\text{KL}}(q_{\text{data},\mathbf{y}}(\mathbf{y}_0 | \mathbf{y}_t) \| q_{\text{data},\mathbf{y}}(\mathbf{y}_0 | \mathbf{g}_{\tilde{\ell}}(\mathbf{y}_t))) \right] = 0, \quad (\text{A3})$$

where $\mathbf{y}_0 \in \mathcal{Y}^{L \times \ell_1}$, $\mathbf{y}_t \in \tilde{\mathcal{Y}}^{L \times \ell_1}$, $\tilde{\ell} = \ell_1$, and the second inequality becomes an equality if and only if Eq. (A3) holds with $\tilde{\ell} = \frac{\ell_2}{\ell_1}$, $\mathbf{y}_0 \in \mathcal{Y}^{L \times \ell_2}$, and $\mathbf{y}_t \in \tilde{\mathcal{Y}}^{L \times \ell_2}$.

Proof. The first inequality $\inf_p \mathcal{L}_{vb} \geq \inf_{p_{\ell_1}} \mathcal{L}_{vb}^{(\ell_1)}$ and the corresponding equality condition (Eq. (A3)) are established in **Proposition A.5** while the second inequality $\inf_{p_{\ell_1}} \mathcal{L}_{vb}^{(\ell_1)} \geq \inf_{p_{\ell_2}} \mathcal{L}_{vb}^{(\ell_2)}$ and the corresponding equality condition are established in **Proposition A.6**. Combining these two results yields the chain of inequalities presented in Eq. (A1). \square

The proof of **Proposition A.5** is organized into three primary steps, as illustrated in Fig. A1:

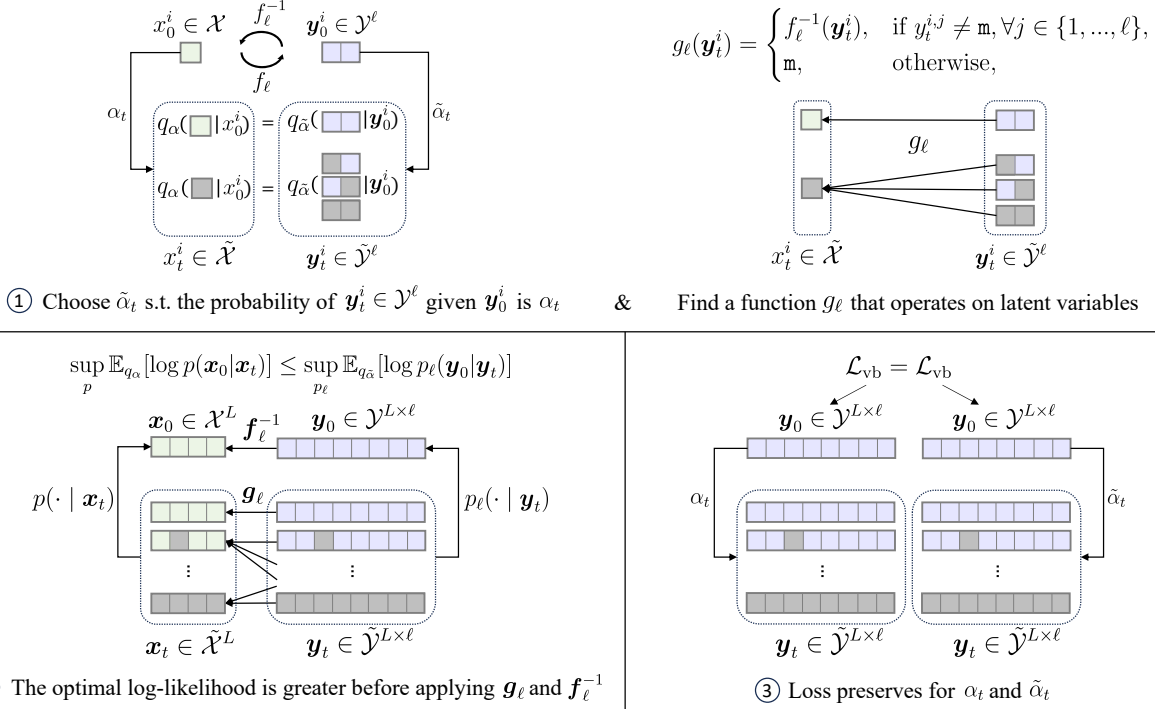


Figure A1. An illustration of the three key steps for proving **Proposition A.5**. Gray tiles represent masked tokens or sub-tokens. Green and purple tiles represent unmasked tokens and sub-tokens, respectively.

- **Step 1:** We identify a scheduling function $\tilde{\alpha}_t$ and a mapping g_ℓ such that the expectations satisfy $\mathbb{E}_{q_\alpha(\mathbf{x}_0, \mathbf{x}_t)}[F(\mathbf{x}_0, \mathbf{x}_t)] = \mathbb{E}_{q_{\tilde{\alpha}}(\mathbf{y}_0, \mathbf{y}_t)}[F(\mathbf{f}_\ell^{-1}(\mathbf{y}_0), \mathbf{g}_\ell(\mathbf{y}_t))]$ for any arbitrary function $F : \mathcal{X}^L \times \tilde{\mathcal{X}}^L \rightarrow \mathbb{R}$. This equivalence is formally established in **Lemma A.2**.
- **Step 2:** We demonstrate that the logarithmic probability of MDM-Prime is point-wisely greater than or equal to that of MDM for every timestep $t \in [0, 1]$. This comparison is detailed in **Lemma A.3**.
- **Step 3:** Finally, we prove that the variational bounds remain invariant under different choices of the scheduling function, as presented in **Lemma A.4**.

By synthesizing these three results, we arrive at the inequality established in the proposition.

Lemma A.2. Let $\mathbf{x}_t \sim q_\alpha(\cdot | \mathbf{x}_0)$ and $\mathbf{y}_t \sim q_{\tilde{\alpha}}(\cdot | \mathbf{y}_0)$, where $\tilde{\alpha}_t \triangleq \alpha_t^{1/\ell}$ and $\mathbf{y}_0 = \mathbf{f}_\ell(\mathbf{x}_0)$. In addition, let $\mathbf{g}_\ell : \tilde{\mathcal{Y}}^{L \times \ell} \rightarrow \tilde{\mathcal{X}}^L$ be a function defined in Eq. (A2). Given any mapping function $F : \mathcal{X}^L \times \tilde{\mathcal{X}}^L \rightarrow \mathbb{R}$, the following equality holds:

$$\mathbb{E}_{q_\alpha(\mathbf{x}_0, \mathbf{x}_t)}[F(\mathbf{x}_0, \mathbf{x}_t)] = \mathbb{E}_{q_{\tilde{\alpha}}(\mathbf{y}_0, \mathbf{y}_t)}[F(\mathbf{f}_\ell^{-1}(\mathbf{y}_0), \mathbf{g}_\ell(\mathbf{y}_t))]. \quad (\text{A4})$$

Proof.

$$\begin{aligned} & \mathbb{E}_{q_{\tilde{\alpha}}(\mathbf{y}_0, \mathbf{y}_t)}[F(\mathbf{f}_\ell^{-1}(\mathbf{y}_0), \mathbf{g}_\ell(\mathbf{y}_t))] \\ & \stackrel{(i)}{=} \mathbb{E}_{q_{\text{data}} \circ \mathbf{f}_\ell^{-1}(\mathbf{y}_0)} \left[\sum_{\mathbf{y}_t} F(\mathbf{f}_\ell^{-1}(\mathbf{y}_0), \mathbf{g}_\ell(\mathbf{y}_t)) q_{\tilde{\alpha}}(\mathbf{y}_t | \mathbf{y}_0) \right] \\ & = \mathbb{E}_{q_{\text{data}} \circ \mathbf{f}_\ell^{-1}(\mathbf{y}_0)} \left[\sum_{\mathbf{y}_t} F(\mathbf{f}_\ell^{-1}(\mathbf{y}_0), \mathbf{g}_\ell(\mathbf{y}_t)) \prod_{i=1}^L \prod_{j=1}^{\ell} q_{\tilde{\alpha}}(y_t^{i,j} | y_0^{i,j}) \right] \\ & \stackrel{(ii)}{=} \mathbb{E}_{q_{\text{data}} \circ \mathbf{f}_\ell^{-1}(\mathbf{y}_0)} \left[\sum_{\mathbf{y}_t} F(\mathbf{f}_\ell^{-1}(\mathbf{y}_0), \mathbf{g}_\ell(\mathbf{y}_t)) \prod_{i=1}^L \prod_{j=1}^{\ell} (1 - \tilde{\alpha}_t) \delta_m(y_t^{i,j}) + \tilde{\alpha}_t \delta_{y_0^i}(y_t^{i,j}) \right] \end{aligned}$$

$$\begin{aligned}
 &= \mathbb{E}_{q_{\text{data}} \circ \mathbf{f}_\ell^{-1}(\mathbf{y}_0)} \left[\sum_{\mathbf{y}_t} F(\mathbf{f}_\ell^{-1}(\mathbf{y}_0), \mathbf{g}_\ell(\mathbf{y}_t)) \prod_{i=1}^L \prod_{j=1}^\ell (1 - \alpha_t^{1/\ell}) \delta_m(\mathbf{y}_t^{i,j}) + \alpha_t^{1/\ell} \delta_{\mathbf{y}_0^{i,j}}(\mathbf{y}_t^{i,j}) \right] \\
 &= \mathbb{E}_{q_{\text{data}} \circ \mathbf{f}_\ell^{-1}(\mathbf{y}_0)} \left[\sum_{\mathbf{y}_t} F(\mathbf{f}_\ell^{-1}(\mathbf{y}_0), \mathbf{g}_\ell(\mathbf{y}_t)) \prod_{i=1}^L (1 - (\alpha_t^{1/\ell})^\ell) \delta_m(\mathbf{y}_t^{i,1}) \cdots \delta_m(\mathbf{y}_t^{i,\ell}) + \cdots + (\alpha_t^{1/\ell})^\ell \delta_{\mathbf{y}_0^{i,1}}(\mathbf{y}_t^{i,1}) \cdots \delta_{\mathbf{y}_0^{i,\ell}}(\mathbf{y}_t^{i,\ell}) \right] \\
 &= \mathbb{E}_{q_{\text{data}} \circ \mathbf{f}_\ell^{-1}(\mathbf{y}_0)} \left[\sum_{\mathbf{y}_t} F(\mathbf{f}_\ell^{-1}(\mathbf{y}_0), \mathbf{g}_\ell(\mathbf{y}_t)) \prod_{i=1}^L (1 - (\alpha_t^{1/\ell})^\ell) \delta_{m, \dots, m}(\mathbf{y}_t^{i,1}, \dots, \mathbf{y}_t^{i,\ell}) + \cdots + (\alpha_t^{1/\ell})^\ell \delta_{\mathbf{y}_0^{i,1}, \dots, \mathbf{y}_0^{i,\ell}}(\mathbf{y}_0^{i,1}, \dots, \mathbf{y}_0^{i,\ell}) \right] \\
 &= \mathbb{E}_{q_{\text{data}} \circ \mathbf{f}_\ell^{-1}(\mathbf{y}_0)} \left[\sum_{\mathbf{y}_t} F(\mathbf{f}_\ell^{-1}(\mathbf{y}_0), \mathbf{g}_\ell(\mathbf{y}_t)) \prod_{i=1}^L (1 - (\alpha_t^{1/\ell})^\ell) \delta_{m, \dots, m}(\mathbf{y}_t^i) + \cdots + (\alpha_t^{1/\ell})^\ell \delta_{\mathbf{y}_0^i}(\mathbf{y}_t^i) \right] \\
 &= \mathbb{E}_{q_{\text{data}}(\mathbf{x}_0)} \left[\sum_{\mathbf{y}_t} F(\mathbf{x}_0, \mathbf{g}_\ell(\mathbf{y}_t)) \prod_{i=1}^L \underbrace{(1 - (\alpha_t^{1/\ell})^\ell) \delta_{m, \dots, m}(\mathbf{y}_t^i)}_{\text{Contains at least one m}} + \underbrace{(\alpha_t^{1/\ell})^\ell \delta_{f_\ell(x_0^i)}(\mathbf{y}_t^i)}_{\text{Contains no m}} \right] \\
 &\stackrel{(iii)}{=} \mathbb{E}_{q_{\text{data}}(\mathbf{x}_0)} \left[\sum_{\mathbf{y}_t} F(\mathbf{x}_0, \mathbf{g}_\ell(\mathbf{y}_t)) \prod_{i=1}^L (1 - (\alpha_t^{1/\ell})^\ell) \delta_m(\mathbf{g}_\ell(\mathbf{y}_t^i)) + (\alpha_t^{1/\ell})^\ell \delta_{x_0^i}(\mathbf{g}_\ell(\mathbf{y}_t^i)) \right] \\
 &= \mathbb{E}_{q_{\text{data}}(\mathbf{x}_0)} \left[\sum_{\mathbf{y}_t} F(\mathbf{x}_0, \mathbf{g}_\ell(\mathbf{y}_t)) \prod_{i=1}^L (1 - \alpha_t) \delta_m(\mathbf{g}_\ell(\mathbf{y}_t^i)) + \alpha_t \delta_{x_0^i}(\mathbf{g}_\ell(\mathbf{y}_t^i)) \right] \\
 &= \mathbb{E}_{q_{\text{data}}(\mathbf{x}_0)} \left[\sum_{\mathbf{y}_t} F(\mathbf{x}_0, \mathbf{g}_\ell(\mathbf{y}_t)) q_\alpha(\mathbf{g}_\ell(\mathbf{y}_t) | \mathbf{x}_0) \right] \\
 &\stackrel{(iv)}{=} \mathbb{E}_{q_{\text{data}}(\mathbf{x}_0)} \left[\sum_{\mathbf{x}_t} F(\mathbf{x}_0, \mathbf{x}_t) q_\alpha(\mathbf{x}_t | \mathbf{x}_0) \right] \\
 &= \mathbb{E}_{q_\alpha(\mathbf{x}_0, \mathbf{x}_t)} [F(\mathbf{x}_0, \mathbf{x}_t)].
 \end{aligned}$$

In step (i), $q_{\tilde{\alpha}}(\mathbf{y}_0, \mathbf{y}_t) = q_{\tilde{\alpha}}(\mathbf{y}_t | \mathbf{y}_0) q_{\text{data}, \mathbf{y}}(\mathbf{y}_0) = q_{\tilde{\alpha}}(\mathbf{y}_t | \mathbf{y}_0) q_{\text{data}} \circ \mathbf{f}_\ell^{-1}(\mathbf{y}_0)$ by definition. In step (ii), $q_{\tilde{\alpha}}(\mathbf{y}_t | \mathbf{y}_0)$ is expanded according to Eq. (4). In step (iii), since F depends on \mathbf{y}_t only through $\mathbf{g}_\ell(\mathbf{y}_t)$, we group terms by their image under \mathbf{g}_ℓ . The domain of \mathbf{y}_t^i partitions into vectors containing at least one m and the fully-unmasked value $f_\ell(x_0^i)$. Their respective probability masses are $1 - (\tilde{\alpha}_t)^\ell = 1 - \alpha_t$ and $(\tilde{\alpha}_t)^\ell = \alpha_t$, yielding the two-term expression in terms of $\mathbf{g}_\ell(\mathbf{y}_t^i)$. In step (iv), the summation is performed on $\mathbf{x}_t \in \tilde{\mathcal{X}}^L$ (i.e., the codomain of \mathbf{g}_ℓ). \square

Lemma A.3. Let $\tilde{\alpha}_t \triangleq \alpha_t^{1/\ell}$. The following inequality holds:

$$\sup_p \mathbb{E}_{q_\alpha(\mathbf{x}_0, \mathbf{x}_t)} [\log p(\mathbf{x}_0 | \mathbf{x}_t)] \leq \sup_{p_\ell} \mathbb{E}_{q_{\tilde{\alpha}}(\mathbf{y}_0, \mathbf{y}_t)} [\log p_\ell(\mathbf{y}_0 | \mathbf{y}_t)], \quad \forall t \in [0, 1]. \quad (\text{A5})$$

The equality holds if and only if:

$$\mathbb{E}_{q_{\tilde{\alpha}}(\mathbf{y}_t)} [\mathbb{D}_{KL}(q_{\text{data}, \mathbf{y}}(\mathbf{y}_0 | \mathbf{y}_t) || q_{\text{data}, \mathbf{y}}(\mathbf{y}_0 | \mathbf{g}_\ell(\mathbf{y}_t))] = 0. \quad (\text{A6})$$

Proof. The proof demonstrates that $\sup_{p_\ell} \mathbb{E}_{q_{\tilde{\alpha}}(\mathbf{y}_0, \mathbf{y}_t)} [\log p_\ell(\mathbf{y}_0 | \mathbf{y}_t)] - \sup_p \mathbb{E}_{q_\alpha(\mathbf{x}_0, \mathbf{x}_t)} [\log p(\mathbf{x}_0 | \mathbf{x}_t)] \geq 0$ by first expanding both terms. $\sup_{p_\ell} \mathbb{E}_{q_{\tilde{\alpha}}(\mathbf{y}_0, \mathbf{y}_t)} [\log p_\ell(\mathbf{y}_0 | \mathbf{y}_t)]$ is expanded as follows:

$$\begin{aligned}
 &\sup_{p_\ell} \mathbb{E}_{q_{\tilde{\alpha}}(\mathbf{y}_0, \mathbf{y}_t)} [\log p_\ell(\mathbf{y}_0 | \mathbf{y}_t)] \\
 &\stackrel{(i)}{=} \sup_{p_\ell} \left(\mathbb{E}_{q_{\tilde{\alpha}}(\mathbf{y}_0, \mathbf{y}_t)} [\log p_\ell(\mathbf{y}_0 | \mathbf{y}_t)] + \mathbb{E}_{q_{\tilde{\alpha}}(\mathbf{y}_0, \mathbf{y}_t)} [\log q_{\text{data}, \mathbf{y}}(\mathbf{y}_0 | \mathbf{y}_t)] - \mathbb{E}_{q_{\tilde{\alpha}}(\mathbf{y}_0, \mathbf{y}_t)} [\log q_{\text{data}, \mathbf{y}}(\mathbf{y}_0 | \mathbf{y}_t)] \right) \\
 &= \sup_{p_\ell} \left(\mathbb{E}_{q_{\tilde{\alpha}}(\mathbf{y}_0, \mathbf{y}_t)} [\log q_{\text{data}, \mathbf{y}}(\mathbf{y}_0 | \mathbf{y}_t)] - \mathbb{E}_{q_{\tilde{\alpha}}(\mathbf{y}_0, \mathbf{y}_t)} \left[\log \frac{q_{\text{data}, \mathbf{y}}(\mathbf{y}_0 | \mathbf{y}_t)}{p_\ell(\mathbf{y}_0 | \mathbf{y}_t)} \right] \right)
 \end{aligned}$$

$$\begin{aligned}
 &= \sup_{p_\ell} \left(\mathbb{E}_{q_{\tilde{\alpha}}(\mathbf{y}_0, \mathbf{y}_t)} [\log q_{\text{data},y}(\mathbf{y}_0 | \mathbf{y}_t) - \mathbb{E}_{q_{\tilde{\alpha}}(\mathbf{y}_t)} \left[\mathbb{E}_{q_{\text{data},y}(\mathbf{y}_0 | \mathbf{y}_t)} \left[\log \frac{q_{\text{data},y}(\mathbf{y}_0 | \mathbf{y}_t)}{p_\ell(\mathbf{y}_0 | \mathbf{y}_t)} \right] \right] \right) \\
 &= \mathbb{E}_{q_{\tilde{\alpha}}(\mathbf{y}_0, \mathbf{y}_t)} [\log q_{\text{data},y}(\mathbf{y}_0 | \mathbf{y}_t)] - \inf_{p_\ell} \mathbb{E}_{q_{\tilde{\alpha}}(\mathbf{y}_t)} \left[\mathbb{D}_{\text{KL}}(q_{\text{data},y}(\mathbf{y}_0 | \mathbf{y}_t) \| p_\ell(\mathbf{y}_0 | \mathbf{y}_t)) \right] \\
 &\stackrel{(ii)}{=} \mathbb{E}_{q_{\tilde{\alpha}}(\mathbf{y}_0, \mathbf{y}_t)} [\log q_{\text{data},y}(\mathbf{y}_0 | \mathbf{y}_t)],
 \end{aligned}$$

where (i) adds and subtracts $\mathbb{E}_{q_{\tilde{\alpha}}(\mathbf{y}_0, \mathbf{y}_t)} [\log q_{\text{data},y}(\mathbf{y}_0 | \mathbf{y}_t)]$, and (ii) shows the optimum that the KL divergence becomes zero (i.e., $p_\ell(\mathbf{y}_0 | \mathbf{y}_t) = q_{\text{data},y}(\mathbf{y}_0 | \mathbf{y}_t)$). On the other hand, $\sup_p \mathbb{E}_{q_\alpha(\mathbf{x}_0, \mathbf{x}_t)} [\log p(\mathbf{x}_0 | \mathbf{x}_t)]$ can be simplified as an expected entropy term by following a similar derivation:

$$\begin{aligned}
 &\sup_p \mathbb{E}_{q_\alpha(\mathbf{x}_0, \mathbf{x}_t)} [\log p(\mathbf{x}_0 | \mathbf{x}_t)] \\
 &= \sup_p \left(\mathbb{E}_{q_\alpha(\mathbf{x}_0, \mathbf{x}_t)} [\log p(\mathbf{x}_0 | \mathbf{x}_t)] + \mathbb{E}_{q_\alpha(\mathbf{x}_0, \mathbf{x}_t)} [\log q_{\text{data}}(\mathbf{x}_0 | \mathbf{x}_t)] - \mathbb{E}_{q_\alpha(\mathbf{x}_0, \mathbf{x}_t)} [\log q_{\text{data}}(\mathbf{x}_0 | \mathbf{x}_t)] \right) \\
 &= \sup_p \left(\mathbb{E}_{q_\alpha(\mathbf{x}_0, \mathbf{x}_t)} [\log q_{\text{data}}(\mathbf{x}_0 | \mathbf{x}_t)] - \mathbb{E}_{q_\alpha(\mathbf{x}_0, \mathbf{x}_t)} \left[\log \frac{q_{\text{data}}(\mathbf{x}_0 | \mathbf{x}_t)}{p(\mathbf{x}_0 | \mathbf{x}_t)} \right] \right) \\
 &= \mathbb{E}_{q_\alpha(\mathbf{x}_0, \mathbf{x}_t)} [\log q_{\text{data}}(\mathbf{x}_0 | \mathbf{x}_t)] - \inf_p \mathbb{E}_{q_\alpha(\mathbf{x}_t)} \left[\mathbb{D}_{\text{KL}}(q_{\text{data}}(\mathbf{x}_0 | \mathbf{x}_t) \| p(\mathbf{x}_0 | \mathbf{x}_t)) \right] \\
 &= \mathbb{E}_{q_\alpha(\mathbf{x}_0, \mathbf{x}_t)} [\log q_{\text{data}}(\mathbf{x}_0 | \mathbf{x}_t)] \\
 &\stackrel{(i)}{=} \mathbb{E}_{q_{\tilde{\alpha}}(\mathbf{y}_0, \mathbf{y}_t)} [\log q_{\text{data}}(\mathbf{f}_\ell^{-1}(\mathbf{y}_0) | \mathbf{g}_\ell(\mathbf{y}_t))],
 \end{aligned}$$

where (i) rewrites the expectation via **Lemma A.2**. Based on the expanded terms, the proof concludes:

$$\begin{aligned}
 &\sup_{p_\ell} \mathbb{E}_{q_{\tilde{\alpha}}(\mathbf{y}_0, \mathbf{y}_t)} [\log p_\ell(\mathbf{y}_0 | \mathbf{y}_t)] - \sup_p \mathbb{E}_{q_\alpha(\mathbf{x}_0, \mathbf{x}_t)} [\log p(\mathbf{x}_0 | \mathbf{x}_t)] \\
 &= \mathbb{E}_{q_{\tilde{\alpha}}(\mathbf{y}_0, \mathbf{y}_t)} [\log q_{\text{data},y}(\mathbf{y}_0 | \mathbf{y}_t)] - \mathbb{E}_{q_{\tilde{\alpha}}(\mathbf{y}_0, \mathbf{y}_t)} [\log q_{\text{data}}(\mathbf{f}_\ell^{-1}(\mathbf{y}_0) | \mathbf{g}_\ell(\mathbf{y}_t))] \\
 &= \mathbb{E}_{q_{\tilde{\alpha}}(\mathbf{y}_0, \mathbf{y}_t)} \left[\log \frac{q_{\text{data},y}(\mathbf{y}_0 | \mathbf{y}_t)}{q_{\text{data}}(\mathbf{f}_\ell^{-1}(\mathbf{y}_0) | \mathbf{g}_\ell(\mathbf{y}_t))} \right] \\
 &= \mathbb{E}_{q_{\tilde{\alpha}}(\mathbf{y}_t)} \left[\mathbb{D}_{\text{KL}}(q_{\text{data},y}(\mathbf{y}_0 | \mathbf{y}_t) \| q_{\text{data}} \circ \mathbf{f}_\ell^{-1}(\mathbf{y}_0 | \mathbf{g}_\ell(\mathbf{y}_t))) \right] \\
 &= \mathbb{E}_{q_{\tilde{\alpha}}(\mathbf{y}_t)} \left[\mathbb{D}_{\text{KL}}(q_{\text{data},y}(\mathbf{y}_0 | \mathbf{y}_t) \| q_{\text{data},y}(\mathbf{y}_0 | \mathbf{g}_\ell(\mathbf{y}_t))) \right] \geq 0.
 \end{aligned}$$

By rearranging the inequality, we conclude that $\sup_{p_\ell} \mathbb{E}_{q_{\tilde{\alpha}}(\mathbf{y}_0, \mathbf{y}_t)} [\log p_\ell(\mathbf{y}_0 | \mathbf{y}_t)] \geq \sup_p \mathbb{E}_{q_\alpha(\mathbf{x}_0, \mathbf{x}_t)} [\log p(\mathbf{x}_0 | \mathbf{x}_t)]$ and the equality holds when $\mathbb{E}_{q_{\tilde{\alpha}}(\mathbf{y}_t)} \left[\mathbb{D}_{\text{KL}}(q_{\text{data},y}(\mathbf{y}_0 | \mathbf{y}_t) \| q_{\text{data},y}(\mathbf{y}_0 | \mathbf{g}_\ell(\mathbf{y}_t))) \right] = 0$. \square

Lemma A.4. (cf. (Sahoo et al., 2024; Shi et al., 2024; Kingma et al., 2021)) Let $\alpha_t, \tilde{\alpha}_t : [0, 1] \rightarrow [1, 0]$ be two strictly decreasing, continuous bijections with $\alpha_0 = \tilde{\alpha}_0 = 1$ and $\alpha_1 = \tilde{\alpha}_1 = 0$. For any function $F : (0, 1) \rightarrow \mathbb{R}$ integrable on $(0, 1)$, define:

$$I(\alpha) \triangleq \int_0^1 \frac{\alpha'_t}{1 - \alpha_t} F(\alpha_t) dt. \quad (\text{A7})$$

Then, we have:

$$I(\alpha) = I(\tilde{\alpha}). \quad (\text{A8})$$

Proof. Let $s = \alpha_t$. Then, $ds = \alpha'_t dt$. As $t : 0 \rightarrow 1$, we have $s : 1 \rightarrow 0$. Hence,

$$I(\alpha) = \int_{t=0}^1 \frac{\alpha'_t}{1 - \alpha_t} F(\alpha_t) dt = \int_{s=1}^0 \frac{1}{1 - s} F(s) ds.$$

Let $s = \tilde{\alpha}_t$. Then, $ds = \tilde{\alpha}'_t dt$. As $s : 1 \rightarrow 0$, we have $t : 0 \rightarrow 1$. Hence,

$$\int_{s=1}^0 \frac{1}{1 - s} F(s) ds = \int_{t=0}^1 \frac{\tilde{\alpha}'_t}{1 - \tilde{\alpha}_t} F(\tilde{\alpha}_t) dt = I(\tilde{\alpha}).$$

Therefore, $I(\alpha) = I(\tilde{\alpha})$. \square

Proposition A.5. *Given a scheduling function α_t , the following inequality holds:*

$$\inf_{p_\ell} \int_0^1 \frac{\alpha'_t}{1 - \alpha_t} \mathbb{E}_{q_\alpha(\mathbf{y}_0, \mathbf{y}_t)} [\log p_\ell(\mathbf{y}_0 | \mathbf{y}_t)] dt \leq \inf_p \int_0^1 \frac{\alpha'_t}{1 - \alpha_t} \mathbb{E}_{q_\alpha(\mathbf{x}_0, \mathbf{x}_t)} [\log p(\mathbf{x}_0 | \mathbf{x}_t)] dt. \quad (\text{A9})$$

The equality holds if and only if:

$$\mathbb{E}_{q_{\tilde{\alpha}}(\mathbf{y}_t)} [\mathbb{D}_{\text{KL}}(q_{\text{data}, \mathbf{y}}(\mathbf{y}_0 | \mathbf{y}_t) \| q_{\text{data}, \mathbf{y}}(\mathbf{y}_0 | \mathbf{g}_\ell(\mathbf{y}_t)))] = 0. \quad (\text{A10})$$

Proof.

$$\begin{aligned} \inf_{p_\ell} \int_0^1 \frac{\alpha'_t}{1 - \alpha_t} \mathbb{E}_{q_\alpha(\mathbf{y}_0, \mathbf{y}_t)} [\log p_\ell(\mathbf{y}_0 | \mathbf{y}_t)] dt &\stackrel{(i)}{=} \int_0^1 \frac{\alpha'_t}{1 - \alpha_t} \sup_{p_\ell} \mathbb{E}_{q_\alpha(\mathbf{y}_0, \mathbf{y}_t)} [\log p_\ell(\mathbf{y}_0 | \mathbf{y}_t)] dt \\ &\stackrel{(ii)}{=} \int_0^1 \frac{\tilde{\alpha}'_t}{1 - \tilde{\alpha}_t} \sup_{p_\ell} \mathbb{E}_{q_{\tilde{\alpha}}(\mathbf{y}_0, \mathbf{y}_t)} [\log p_\ell(\mathbf{y}_0 | \mathbf{y}_t)] dt \\ &\stackrel{(iii)}{\leq} \int_0^1 \frac{\alpha'_t}{1 - \alpha_t} \sup_p \mathbb{E}_{q_\alpha(\mathbf{x}_0, \mathbf{x}_t)} [\log p(\mathbf{x}_0 | \mathbf{x}_t)] dt \\ &= \inf_p \int_0^1 \frac{\alpha'_t}{1 - \alpha_t} \mathbb{E}_{q_\alpha(\mathbf{x}_0, \mathbf{x}_t)} [\log p(\mathbf{x}_0 | \mathbf{x}_t)] dt, \end{aligned}$$

where (i) is due to $\frac{\alpha'_t}{1 - \alpha_t} < 0$, (ii) is due to **Lemma A.4**, and (iii) is due to **Lemma A.3**. The equality holds if and only if $\mathbb{E}_{q_{\tilde{\alpha}}(\mathbf{y}_t)} [\mathbb{D}_{\text{KL}}(q_{\text{data}, \mathbf{y}}(\mathbf{y}_0 | \mathbf{y}_t) \| q_{\text{data}, \mathbf{y}}(\mathbf{y}_0 | \mathbf{g}_\ell(\mathbf{y}_t)))] = 0$ according to **Lemma A.3**. \square

Lemmas A.2-A.4 and **Proposition A.5** show that if the scheduling $\tilde{\alpha}_t$ and the corresponding mapping \mathbf{g}_ℓ can be identified, the inequality in Eq. (A9) can be successfully established. We follow the same rationale to examine an additional extended theory: as the token granularity ℓ grows larger, the bound gets tighter. **Proposition A.6** generalizes **Proposition A.5** to compare the optimal losses of two MDM-Prime models with different token granularities.

Let ℓ_1 and ℓ_2 denote token granularities. We define $\mathbf{y}_0^{(\ell_1)} \triangleq \mathbf{f}_{\ell_1}(\mathbf{x}_0) \in \mathcal{Y}_1^{L \times \ell_1}$ and $\mathbf{y}_0^{(\ell_2)} \triangleq \mathbf{f}_{\ell_2}(\mathbf{x}_0) \in \mathcal{Y}_2^{L \times \ell_2}$, where the target spaces are defined as $\mathcal{Y}_k = \{0, \dots, \lceil \sqrt[\ell_k]{V} \rceil - 1\}$ for $k \in \{1, 2\}$. For notational simplicity, we represent the distribution of $\mathbf{y}_0^{(\ell_2)}$ as $q_{\text{data}, \mathbf{y}}(\mathbf{y}_0^{(\ell_2)})$ without explicitly defining a separate distribution symbol for $\mathbf{y}_0^{(\ell_1)}$.

We further specify the mappings $\mathbf{f}_{\tilde{\ell}}$ and $\mathbf{g}_{\tilde{\ell}}$ (Eq. (A2)) for transitioning between granularities with ratio $\tilde{\ell} = \ell_2 / \ell_1$. First, $\mathbf{f}_{\tilde{\ell}} : \mathcal{Y}_1^{L \times \ell_1} \rightarrow \mathcal{Y}_2^{L \times \ell_2}$ is an invertible function defined by the element-wise operation $f_{\tilde{\ell}} : \mathcal{Y}_1 \rightarrow \mathcal{Y}_2^{\tilde{\ell}}$. We denote the mapping of a sequence as $\mathbf{y}_0^{(\ell_2)} = \mathbf{f}_{\tilde{\ell}}(\mathbf{y}_0^{(\ell_1)})$. With this definition, $\mathbf{y}_0^{(\ell_2)}$ can be expanded as follows:

$$\begin{aligned} \mathbf{y}_0^{(\ell_2)} = \mathbf{f}_{\tilde{\ell}}(\mathbf{y}_0^{(\ell_1)}) &= [f_{\tilde{\ell}}(\mathbf{y}_0^{(\ell_1), i, 1}), \dots, f_{\tilde{\ell}}(\mathbf{y}_0^{(\ell_1), i, \ell_1})] \\ &= [\mathbf{y}_0^{(\ell_2), i, 1}, \dots, \mathbf{y}_0^{(\ell_2), i, \ell_1}] \\ &= [(y_0^{(\ell_2), i, 1}, \dots, y_0^{(\ell_2), i, \tilde{\ell}}), \dots, (y_0^{(\ell_2), i, \tilde{\ell}(\ell_1 - 1)}, \dots, y_0^{(\ell_2), i, \ell_2})]. \end{aligned}$$

Second, the function $\mathbf{g}_{\tilde{\ell}}$ is defined by the element-wise operation $g_{\tilde{\ell}}$. This function applies the inverse mapping $f_{\tilde{\ell}}^{-1}$ only if all corresponding sub-tokens are unmasked. Otherwise, it returns the masked token m . The definition aligns with Eq. (A2) as follows:

$$g_{\frac{\ell_2}{\ell_1}}(\mathbf{y}_t^{(\ell_2), i, j}) = \begin{cases} f_{\frac{\ell_2}{\ell_1}}^{-1}(\mathbf{y}_t^{(\ell_2), i, j}), & \text{if } y_t^{i, \frac{\ell_2}{\ell_1}(j-1)+k} \neq m, \forall k \in \{1, \dots, \frac{\ell_2}{\ell_1}\}, \\ m, & \text{otherwise.} \end{cases}$$

Proposition A.6. *Let ℓ_1, ℓ_2 be token granularities satisfying $1 < \ell_1 < \ell_2$ and $\frac{\ell_2}{\ell_1} \in \mathbb{N}$. Then, the optimal variational bound is monotone with respect to the token granularity:*

$$\inf_{p_{\ell_2}} \int_0^1 \frac{\alpha'_t}{1 - \alpha_t} \mathbb{E}_{q_\alpha(\mathbf{y}_0^{(\ell_2)}, \mathbf{y}_t^{(\ell_2)})} [\log p_{\ell_2}(\mathbf{y}_0^{(\ell_2)} | \mathbf{y}_t^{(\ell_2)})] dt \leq \inf_{p_{\ell_1}} \int_0^1 \frac{\alpha'_t}{1 - \alpha_t} \mathbb{E}_{q_\alpha(\mathbf{y}_0^{(\ell_1)}, \mathbf{y}_t^{(\ell_1)})} [\log p_{\ell_1}(\mathbf{y}_0^{(\ell_1)} | \mathbf{y}_t^{(\ell_1)})] dt. \quad (\text{A11})$$

The equality holds if and only if:

$$\mathbb{E}_{q_{\tilde{\alpha}}(\mathbf{y}_t^{(\ell_2)})} \left[\mathbb{D}_{\text{KL}}(q_{\text{data},y}(\mathbf{y}_0^{(\ell_2)} | \mathbf{y}_t^{(\ell_2)}) \| q_{\text{data},y}(\mathbf{y}_0^{(\ell_2)} | \mathbf{g}_{\tilde{\ell}_1}(\mathbf{y}_t^{(\ell_2)}))) \right] = 0. \quad (\text{A12})$$

Proof. The proof first identifies the transformation between $\mathbf{y}_0^{(\ell_1)}$ and $\mathbf{y}_0^{(\ell_2)}$. Then, it establishes the inequality by following the proof presented in **Proposition A.5**.

Given that $\tilde{\ell} = \frac{\ell_2}{\ell_1}$, the invertible transformation \mathbf{f}_{ℓ_2} can be decomposed as $\mathbf{f}_{\ell_2} = \mathbf{f}_{\tilde{\ell}} \circ \mathbf{f}_{\ell_1}$, and $\mathbf{y}_0^{(\ell_2)}$ can be derived through $\mathbf{y}_0^{(\ell_1)}$ according to $\mathbf{y}_0^{(\ell_2)} = \mathbf{f}_{\tilde{\ell}}(\mathbf{y}_0^{(\ell_1)})$. In addition, let $\tilde{\alpha}_t = \alpha_t^{1/\tilde{\ell}}$. We can establish analogues to **Lemma A.2** and **Lemma A.3** using the same derivation steps:

$$\begin{aligned} \mathbb{E}_{q_{\alpha}(\mathbf{y}_0^{(\ell_1)}, \mathbf{y}_t^{(\ell_1)})} [F(\mathbf{y}_0^{(\ell_1)}, \mathbf{y}_t^{(\ell_1)})] &= \mathbb{E}_{q_{\tilde{\alpha}}(\mathbf{y}_0^{(\ell_2)}, \mathbf{y}_t^{(\ell_2)})} [F(\mathbf{f}_{\tilde{\ell}}^{-1}(\mathbf{y}_0^{(\ell_2)}), \mathbf{g}_{\tilde{\ell}}(\mathbf{y}_t^{(\ell_2)}))]. \\ \sup_{p_{\ell_1}} \mathbb{E}_{q_{\alpha}(\mathbf{y}_0^{(\ell_1)}, \mathbf{y}_t^{(\ell_1)})} [\log p_{\ell_1}(\mathbf{y}_0^{(\ell_1)} | \mathbf{y}_t^{(\ell_1)})] &\leq \sup_{p_{\ell_2}} \mathbb{E}_{q_{\tilde{\alpha}}(\mathbf{y}_0^{(\ell_2)}, \mathbf{y}_t^{(\ell_2)})} [\log p_{\ell_2}(\mathbf{y}_0^{(\ell_2)} | \mathbf{y}_t^{(\ell_2)})], \quad \forall t \in [0, 1]. \end{aligned}$$

Finally, following the derivation of **Proposition A.5**, we have:

$$\begin{aligned} \inf_{p_{\ell_2}} \int_0^1 \frac{\alpha'_t}{1 - \alpha_t} \mathbb{E}_{q_{\alpha}(\mathbf{y}_0^{(\ell_2)}, \mathbf{y}_t^{(\ell_2)})} [\log p_{\ell_2}(\mathbf{y}_0^{(\ell_2)} | \mathbf{y}_t^{(\ell_2)})] dt \\ &= \int_0^1 \frac{\alpha'_t}{1 - \alpha_t} \sup_{p_{\ell_2}} \mathbb{E}_{q_{\alpha}(\mathbf{y}_0^{(\ell_2)}, \mathbf{y}_t^{(\ell_2)})} [\log p_{\ell_2}(\mathbf{y}_0^{(\ell_2)} | \mathbf{y}_t^{(\ell_2)})] dt \\ &= \int_0^1 \frac{\tilde{\alpha}'_t}{1 - \tilde{\alpha}_t} \sup_{p_{\ell_2}} \mathbb{E}_{q_{\tilde{\alpha}}(\mathbf{y}_0^{(\ell_2)}, \mathbf{y}_t^{(\ell_2)})} [\log p_{\ell_2}(\mathbf{y}_0^{(\ell_2)} | \mathbf{y}_t^{(\ell_2)})] dt \\ &\leq \int_0^1 \frac{\alpha'_t}{1 - \alpha_t} \sup_{p_{\ell_1}} \mathbb{E}_{q_{\alpha}(\mathbf{y}_0^{(\ell_1)}, \mathbf{y}_t^{(\ell_1)})} [\log p_{\ell_1}(\mathbf{y}_0^{(\ell_1)} | \mathbf{y}_t^{(\ell_1)})] dt \\ &= \inf_{p_{\ell_1}} \int_0^1 \frac{\alpha'_t}{1 - \alpha_t} \mathbb{E}_{q_{\alpha}(\mathbf{y}_0^{(\ell_1)}, \mathbf{y}_t^{(\ell_1)})} [\log p_{\ell_1}(\mathbf{y}_0^{(\ell_1)} | \mathbf{y}_t^{(\ell_1)})] dt. \end{aligned}$$

The equality holds if and only if $\mathbb{E}_{q_{\tilde{\alpha}}(\mathbf{y}_t^{(\ell_2)})} \left[\mathbb{D}_{\text{KL}}(q_{\text{data},y}(\mathbf{y}_0^{(\ell_2)} | \mathbf{y}_t^{(\ell_2)}) \| q_{\text{data},y}(\mathbf{y}_0^{(\ell_2)} | \mathbf{g}_{\tilde{\ell}}(\mathbf{y}_t^{(\ell_2)}))) \right] = 0. \quad \square$

A.1.2. PROOFS OF PROPOSITIONS 3.3 AND 3.4

As discussed in Section 3.2, the design of the subtokenizer \mathbf{f}_{ℓ} is critical for tightening the variational bound. In this section, we provide the theoretical justifications for **Propositions 3.3** and **3.4**. We begin by deriving **Lemmas A.7-A.8**, which lead to the formulation of **Proposition 3.3**.

Lemma A.7. *The following equality holds:*

$$\mathbb{E}_{q_{\text{data},y}(\mathbf{y}_0)} [\log q_{\text{data},y}(\mathbf{y}_0)] = \mathbb{E}_{q_{\text{data}}(\mathbf{x}_0)} [\log q_{\text{data}}(\mathbf{x}_0)]. \quad (\text{A13})$$

Proof.

$$\begin{aligned} \mathbb{E}_{q_{\text{data}}(\mathbf{x}_0)} [\log q_{\text{data}}(\mathbf{x}_0)] &= \sum_{\mathbf{x}_0} q_{\text{data}}(\mathbf{x}_0) \log q_{\text{data}}(\mathbf{x}_0) \\ &= \sum_{\mathbf{y}_0} q_{\text{data}} \circ \mathbf{f}_{\ell}^{-1}(\mathbf{y}_0) \log q_{\text{data}} \circ \mathbf{f}_{\ell}^{-1}(\mathbf{y}_0) \\ &= \mathbb{E}_{q_{\text{data},y}(\mathbf{y}_0)} [\log q_{\text{data},y}(\mathbf{y}_0)]. \end{aligned}$$

\square

Lemma A.8. *The following equality holds:*

$$\mathbb{E}_{q_{\alpha}(\mathbf{y}_0, \mathbf{y}_t)} [\log q_{\alpha}(\mathbf{y}_t | \mathbf{y}_0)] = L\ell((1 - \alpha_t) \log(1 - \alpha_t) + \alpha_t \log \alpha_t) \quad (\text{A14})$$

Proof.

$$\begin{aligned}
 \mathbb{E}_{q_\alpha(\mathbf{y}_0, \mathbf{y}_t)}[\log q_\alpha(\mathbf{y}_t | \mathbf{y}_0)] &= \mathbb{E}_{q_\alpha(\mathbf{y}_0, \mathbf{y}_t)} \left[\log \left(\prod_{i=1}^L \prod_{j=1}^\ell q_\alpha(y_t^{i,j} | y_0^{i,j}) \right) \right] \\
 &= \sum_{i=1}^L \sum_{j=1}^\ell \mathbb{E}_{q_\alpha(\mathbf{y}_0, \mathbf{y}_t)} \left[\log q_\alpha(y_t^{i,j} | y_0^{i,j}) \right] \\
 &= \sum_{i=1}^L \sum_{j=1}^\ell \mathbb{E}_{q_\alpha(\mathbf{y}_0, \mathbf{y}_t)} \left[\log \left((1 - \alpha_t) \delta_m(y_t^{i,j}) + \alpha_t \delta_{y_0^{i,j}}(y_t^{i,j}) \right) \right] \\
 &\stackrel{(i)}{=} \sum_{i=1}^L \sum_{j=1}^\ell ((1 - \alpha_t) \log(1 - \alpha_t) + \alpha_t \log \alpha_t) \\
 &= L\ell ((1 - \alpha_t) \log(1 - \alpha_t) + \alpha_t \log \alpha_t),
 \end{aligned}$$

where (i) is because $y_t^{i,j} = m$ with probability $1 - \alpha_t$ while $y_t^{i,j} = y_0^{i,j}$ with probability α_t (cf. **Proposition A2** in (Chao et al., 2025)). \square

Proposition 3.3. The optimal variational bound (Eq. (5)) can be decomposed into an f_ℓ -independent and an f_ℓ -dependent term as follows:

$$\inf_{f_\ell} \inf_{p_\ell} \mathcal{L}_{\text{vb}}^{(\ell)} = \int_0^1 \frac{\alpha'_t}{1 - \alpha_t} \left(\underbrace{-\mathcal{H}(\mathbf{y}_0, \mathbf{y}_t)}_{\text{Independent on } f_\ell} + \sup_{f_\ell} \underbrace{\mathcal{H}(\mathbf{y}_t)}_{\text{Dependent on } f_\ell} \right) dt, \quad (\text{A15})$$

where $\mathcal{H}(\mathbf{y}_t) \triangleq \mathbb{E}_{q_\alpha(\mathbf{y}_t)}[-\log q_\alpha(\mathbf{y}_t)]$ and $\mathcal{H}(\mathbf{y}_0, \mathbf{y}_t) \triangleq \mathbb{E}_{q_\alpha(\mathbf{y}_0, \mathbf{y}_t)}[-\log q_\alpha(\mathbf{y}_0, \mathbf{y}_t)]$ represent the entropy of \mathbf{y}_t and the joint entropy of $\mathbf{y}_0, \mathbf{y}_t$, respectively.

Proof.

$$\begin{aligned}
 \inf_{f_\ell} \inf_{p_\ell} \mathcal{L}_{\text{vb}}^{(\ell)} &= \inf_{f_\ell} \inf_{p_\ell} \int_0^1 \frac{\alpha'_t}{1 - \alpha_t} \mathbb{E}_{q_\alpha(\mathbf{y}_0, \mathbf{y}_t)}[\log p_\ell(\mathbf{y}_0 | \mathbf{y}_t)] dt \\
 &\stackrel{(i)}{=} \inf_{f_\ell} \int_0^1 \frac{\alpha'_t}{1 - \alpha_t} \mathbb{E}_{q_\alpha(\mathbf{y}_0, \mathbf{y}_t)}[\log q_{\text{data}, \mathbf{y}}(\mathbf{y}_0 | \mathbf{y}_t)] dt \\
 &\stackrel{(ii)}{=} \int_0^1 \frac{\alpha'_t}{1 - \alpha_t} \sup_{f_\ell} \mathbb{E}_{q_\alpha(\mathbf{y}_0, \mathbf{y}_t)}[\log q_{\text{data}, \mathbf{y}}(\mathbf{y}_0 | \mathbf{y}_t)] dt \\
 &= \int_0^1 \frac{\alpha'_t}{1 - \alpha_t} \sup_{f_\ell} \left(\mathbb{E}_{q_\alpha(\mathbf{y}_0, \mathbf{y}_t)}[\log q_{\text{data}, \mathbf{y}}(\mathbf{y}_0) + \log q_\alpha(\mathbf{y}_t | \mathbf{y}_0) - \log q_\alpha(\mathbf{y}_t)] \right) dt \\
 &= \int_0^1 \frac{\alpha'_t}{1 - \alpha_t} \left(\underbrace{\mathbb{E}_{q_{\text{data}, \mathbf{y}}(\mathbf{y}_0)}[\log q_{\text{data}, \mathbf{y}}(\mathbf{y}_0)]}_{(1) \text{ Independent on } f_\ell} + \underbrace{\mathbb{E}_{q_\alpha(\mathbf{y}_0, \mathbf{y}_t)}[\log q_\alpha(\mathbf{y}_t | \mathbf{y}_0)]}_{(2) \text{ Independent on } f_\ell} + \sup_{f_\ell} \underbrace{\mathbb{E}_{q_\alpha(\mathbf{y}_t)}[-\log q_\alpha(\mathbf{y}_t)]}_{(3) \text{ dependent on } f_\ell} \right) dt \\
 &= \int_0^1 \frac{\alpha'_t}{1 - \alpha_t} \left(\mathbb{E}_{q_\alpha(\mathbf{y}_0, \mathbf{y}_t)}[\log q_\alpha(\mathbf{y}_0, \mathbf{y}_t)] + \sup_{f_\ell} \mathbb{E}_{q_\alpha(\mathbf{y}_t)}[-\log q_\alpha(\mathbf{y}_t)] \right) dt, \\
 &= \int_0^1 \frac{\alpha'_t}{1 - \alpha_t} \left(\underbrace{-\mathcal{H}(\mathbf{y}_0, \mathbf{y}_t)}_{\text{Independent on } f_\ell} + \sup_{f_\ell} \underbrace{\mathcal{H}(\mathbf{y}_t)}_{\text{Dependent on } f_\ell} \right) dt,
 \end{aligned}$$

where (i) is derived in **Lemma A.3** and (ii) follows from the fact that $\frac{\alpha'_t}{1 - \alpha_t} < 0$. Term (1) corresponds to the negative data entropy, $-\mathcal{H}(\mathbf{x}_0) \triangleq \mathbb{E}_{q_{\text{data}}(\mathbf{x}_0)}[\log q_{\text{data}}(\mathbf{x}_0)]$, which is independent of f_ℓ according to **Lemma A.7**. Term (2) represents the negative conditional entropy, $-\mathcal{H}(\mathbf{y}_t | \mathbf{y}_0)$, which equals to the constant $-L\ell[(1 - \alpha_t) \log(1 - \alpha_t) + \alpha_t \log \alpha_t]$ by **Lemma A.8**. Finally, term (3) is $\mathcal{H}(\mathbf{y}_t)$ and is the only component dependent on f_ℓ , making it the primary target of the optimization objective. \square

Next, we show that the entropy of \mathbf{y}_t is bounded. We first present **Lemma A.9** from (Austin et al., 2021; Chao et al., 2025). Then, we provide the proof of **Proposition 3.4**.

Lemma A.9. (cf. Proposition A2 in (Chao et al., 2025))

$$\mathcal{H}(y_t^{i,j}) = \alpha_t \mathcal{H}(y_0^{i,j}) - (1 - \alpha_t) \log(1 - \alpha_t) - \alpha_t \log \alpha_t. \quad (\text{A16})$$

Proof. Please see Eq. (A12) in (Chao et al., 2025) and Section A7 of (Austin et al., 2021). \square

Proposition 3.4. The entropy of \mathbf{y}_t is bounded:

$$\mathcal{H}(\mathbf{y}_t) \leq L\ell(h(\alpha_t) + \alpha_t \log b), \quad (\text{A17})$$

where $h(\alpha_t) = -(1 - \alpha_t) \log(1 - \alpha_t) - \alpha_t \log \alpha_t$. The equality holds if and only if each unmasked $y_t^{i,j}$ is uniformly distributed on \mathcal{Y} .

Proof.

$$\begin{aligned} \mathcal{H}(\mathbf{y}_t) &\stackrel{(i)}{\leq} \sum_{i=1}^L \sum_{j=1}^{\ell} \mathcal{H}(y_t^{i,j}) \\ &\stackrel{(ii)}{=} \sum_{i=1}^L \sum_{j=1}^{\ell} \left(\alpha_t \mathcal{H}(y_0^{i,j}) - (1 - \alpha_t) \log(1 - \alpha_t) - \alpha_t \log \alpha_t \right) \\ &\stackrel{(iii)}{\leq} \sum_{i=1}^L \sum_{j=1}^{\ell} \left(\alpha_t \log b - (1 - \alpha_t) \log(1 - \alpha_t) - \alpha_t \log \alpha_t \right) \\ &= L\ell \left(\alpha_t \log b - (1 - \alpha_t) \log(1 - \alpha_t) - \alpha_t \log \alpha_t \right) \\ &= L\ell \left(\alpha_t \log b + h(\alpha_t) \right), \end{aligned}$$

where (i) is due to the subadditivity of entropy, (ii) is due to **Lemma A.9**, and (iii) is because $|\mathcal{Y}| = b$. The equality holds when each sub-token is independent and uniformly distributed. \square

A.2. Technical Specifications

This section provides further implementation details for the proposed framework. Section A.2.1 describes the architectures of MDM, MDM-Prime, and MDM-Prime-v2, while Section A.2.2 details a practical implementation of the subtokenizer f_ℓ .

A.2.1. MODEL ARCHITECTURE OF MDM-PRIME AND MDM-PRIME-V2

Fig. A2 (a) compares the architectures of MDM, MDM-Prime, and MDM-Prime-v2. MDM-Prime and MDM-Prime-v2 share exactly the same architecture. As detailed in Section 2.2, transitioning from MDM to MDM-Prime (or MDM-Prime-v2) requires only a simple modification of the embedding table (Chao et al., 2025). In this setup, sub-token embeddings are aggregated into token embeddings, and the neural network (i.e., Transformer (θ) in the figure) subsequently processes at the token level. The decoder maintains its original dimensionality to effectively model intra-token dependencies. Specifically, let H represent the hidden layer embedding size of the transformer. The transformers in both architectures accept inputs of size $\mathbb{R}^{H \times L}$ and outputs logits with $\mathbb{R}^{C \times L}$. This design maintains the core model architecture and ensures that the computational cost (FLOPs) per forward pass remains unchanged.

A.2.2. SUBTOKENIZER IMPLEMENTATION

Fig. A2 (b) depicts how the element-wise operation $f_\ell = f_{\text{base-}b} \circ f_{\text{shuffle}}$ of subtokenizer f_ℓ is implemented in practice. This element-wise operation relies on lookup tables: to transform a token x_0^i into a sub-token sequence \mathbf{y}_0^i , the function sequentially retrieves the shuffled index and its corresponding base- b representation. Similarly, the inverse operation f_ℓ^{-1} is executed via a reverse lookup. Both directions can be efficiently implemented using dictionaries in Python.

Please note that the f_ℓ is static over training, and the lookup tables for index shuffling and base- b encoding are also fixed prior to training. In Section A.4, we show that the performance of MDM-Prime-v2 is robust to the choice of the random seed used for the index shuffling operation.

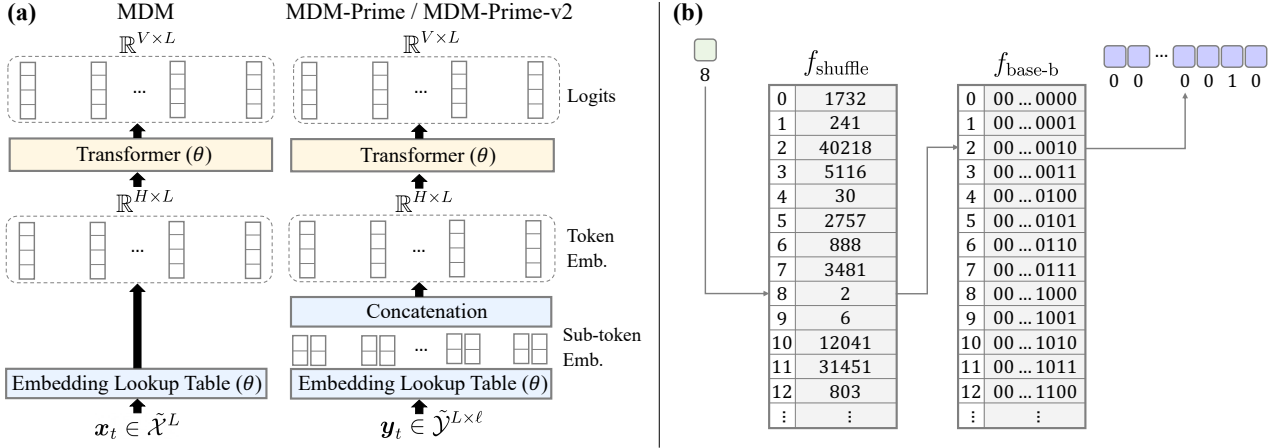


Figure A2. (a) Comparison of MDM, MDM-Prime, and MDM-Prime-v2 architectures. V denotes the vocabulary size, L is the sequence length, ℓ is the token granularity, and H is the Transformer hidden embedding dimension. (b) Implementation of the subtokenizer $f_\ell = f_{\text{base-b}} \circ f_{\text{shuffle}}$. The process utilizes two lookup tables to map indices efficiently; the inverse operation f_ℓ^{-1} is performed by reversing the lookup sequence.

We do not recommend parameterizing and iteratively updating the subtokenizer during training for two reasons. First, our analysis in Section 3.2 suggests that a non-learnable index shuffling operation is sufficiently effective and the sub-token entropy is near the theoretical maximum. Introducing an additional optimization phase for the subtokenizer is likely to yield only marginal gains while significantly increasing computational overhead. Second, updating f_ℓ during training would induce a continuous shift in both the target distribution $q_{\text{data},y}(\mathbf{y}_0)$ and the latent distribution $q_\alpha(\mathbf{y}_t)$. This non-stationarity in the learning objective can result in severe training instability.

A.3. Experimental Configurations

This section provides supplemental experimental details and hyperparameter configurations. The settings for the experiments described in Sections 4.1, 4.2, and 4.3 are detailed in Sections A.3.1, A.3.2, and A.3.3, respectively.

A.3.1. EXPERIMENTS IN SECTION 4.1

Dataset and Preprocessing Method. The training is performed on the C4 dataset (Raffel et al., 2020). Text data is tokenized using the GPT-2 tokenizer (Radford et al., 2019). The maximum sequence length L and the vocabulary size V are defined as 2,048 and 50,257, respectively. The documents are concatenated with the $\langle \text{eod} \rangle$ token as a separator and then wrapped into samples of length 2,048.

Training Configuration. Following prior work (Ni et al., 2025), we employ a Transformer architecture (Vaswani et al., 2017) incorporating Rotary Positional Embeddings (RoPE) (Su et al., 2023), SwiGLU activation (Shazeer, 2020), RMSNorm (Zhang & Sennrich, 2019), and QK-normalization (Dehghani et al., 2023). Model sizes (N) range from 14M to 3.4B parameters; detailed specifications for depth, hidden dimensions, and attention heads are summarized in Table A2. We utilize

Table A2. Model architecture configurations. N represents the number of non-embedding parameters, H denotes the hidden dimension size, B is the number of Transformer blocks, and ‘Heads’ refer to the number of attention heads.

N	H	B	Heads	N	H	B	Heads
14M	448	6	7	252M	1,024	20	16
25M	512	8	8	354M	1,280	18	10
36M	576	9	9	413M	1,280	21	10
49M	640	10	10	571M	1,408	24	11
64M	640	13	10	771M	1,792	20	14
79M	640	16	10	1,107M	2,048	22	16
106M	768	15	12	1,529M	2,304	24	18
154M	896	16	14	2,359M	2,560	30	20
201M	1,024	16	16	3,426M	2,816	36	22

Table A3. Regression parameters for ARM, MDM, and MDM-Prime-v2 fitted according to Chinchilla’s scaling laws (Hoffmann et al., 2022). E denotes the irreducible loss (entropy of the natural text distribution). The terms $A \times N^{-\alpha}$ and $B \times D^{-\beta}$ account for errors arising from finite model size and limited training tokens, respectively.

	ARM	MDM	MDM-Prime-v2
α	0.35	0.35	0.37
β	0.28	0.26	0.26
A	400.0	400.0	400.0
B	400.0	400.0	400.0
E	1.97	2.23	1.30

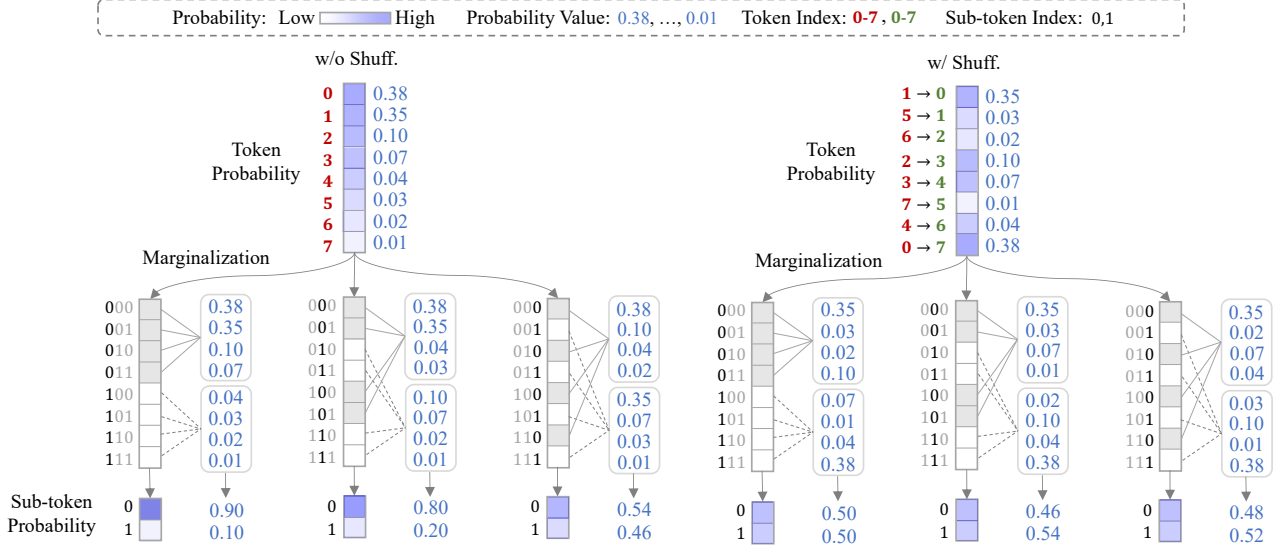


Figure A3. A detailed numerical example of Fig. 3 (a). In this plot, $V = 8$, $\ell = 3$ and $b = 2$. Color intensity represents probability values, where darker blue denotes higher probability. Marginalization is performed by summing entries corresponding to sub-token indices 0 (gray) and 1 (white), respectively. Sub-tokens encoded from standard indices with a structured distribution exhibit low entropy, while the shuffle operation results in sub-tokens with higher entropy.

a linear scheduling function $\alpha_t = 1 - t$ for the diffusion process. Optimization is performed using AdamW (Loshchilov & Hutter, 2019) with $\beta_1 = 0.9$ and $\beta_2 = 0.999$. The learning rate is set to 2×10^{-4} with a cosine decay to a minimum of 2×10^{-5} . We use a batch size of 256 for $N \leq 1.5\text{B}$ and 512 for larger models. The coding framework is based on Megatron-LM (Shoeybi et al., 2019). For hardware, models with $N \leq 400\text{M}$ are trained on eight NVIDIA L40 GPUs (48 GB), while larger models ($N > 400\text{M}$) are trained on eight NVIDIA H100 GPUs (80 GB).

A.3.2. EXPERIMENTS IN SECTION 4.2

Dataset and Preprocessing Method. Training is conducted on the OpenWebText (OWT) dataset (Gokaslan et al., 2019), with text tokenized using the GPT-2 tokenizer (Radford et al., 2019). The maximum sequence length L is set to 1,024, and the vocabulary size V is 50,257. For documents exceeding L , we follow a standard packing procedure: sequences are concatenated using the $\langle \text{eos} \rangle$ token as a delimiter and subsequently partitioned into segments of length 1,024. Each individual sequence is prepended and appended with the $\langle \text{eos} \rangle$ token to mark document boundaries.

Evaluation Method. As OWT does not provide an official validation set, we follow the protocol established by (Sahoo et al., 2024) and reserve the final 100,000 samples for validation. This data preprocessing and evaluation pipeline remains consistent with (Sahoo et al., 2024) to ensure a fair comparison.

Training and Implementation Details. Following previous research (Lou et al., 2024; Sahoo et al., 2024; Shi et al., 2024; Xu et al., 2025; Arriola et al., 2025), we employ a Diffusion Transformer (DiT) architecture (Peebles & Xie, 2022) integrated with RoPE (Su et al., 2023). A detailed configuration of the model architecture adopted in this paper is shown in Table A4. We apply a dropout rate of 0.1 throughout training and utilize a linear scheduling function, $\alpha_t = 1 - t$, for the diffusion process. Optimization is performed using the AdamW optimizer (Loshchilov & Hutter, 2019) with hyperparameters $\beta_1 = 0.9$ and $\beta_2 = 0.999$. The learning rate follows a linear warm-up from 0 to 3×10^{-4} . Training was conducted on eight NVIDIA H100 GPUs, each with 80 GB of memory.

Table A4. DiT model architecture configurations. N represents the number of non-embedding parameters, H denotes the hidden dimension size, B is the number of Transformer blocks, and ‘Heads’ refer to the number of attention heads.

N	H	B	Heads
92M	768	12	12
286M	960	24	16
375M	1024	28	16
860M	1728	24	16

A.3.3. EXPERIMENTS IN SECTION 4.3

Dataset and Preprocessing Method. Following TinyLLaMA (Zhang et al., 2024) and SMDM (Nie et al., 2025a), training is conducted on the SlimPajama dataset (Soboleva et al., 2023), with text tokenized using the LLaMA tokenizer. The

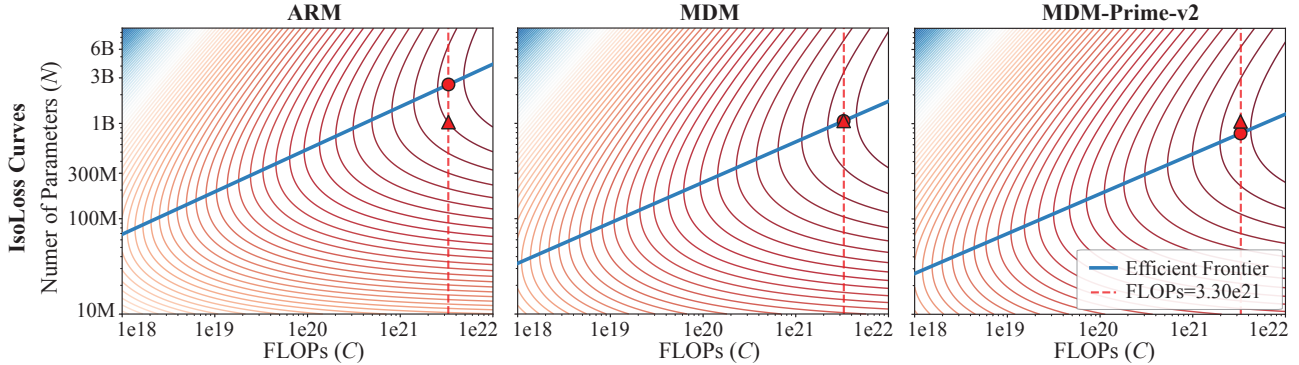


Figure A4. IsoLoss curves for ARM, MDM, and MDM-Prime-v2. The solid blue line denotes the efficient frontier, and the red dashed line represents the 3.3×10^{21} FLOPs setup adopted in Section 4.3. Triangular markers represent the configuration used by SMDM (Nie et al., 2025a) and TinyLLaMA (Zhang et al., 2024), while circular markers denote the compute-optimal setup.

Table A5. An overview of the commonsense reasoning benchmarks used for evaluation.

Benchmark	Description
SciQ	A collection of crowdsourced multiple-choice science exam questions covering Biology, Chemistry, and Physics.
SocialIQA	A large-scale benchmark testing understanding of social interactions, emotional reactions, and motivations.
McTaco	A dataset focusing on temporal commonsense reasoning, requiring answers about duration, frequency, and event ordering.
TruthfulQA	A benchmark measuring whether models mimic human falsehoods, focusing on misconceptions and superstitions.
BoolQ	Naturally occurring yes/no questions paired with Wikipedia paragraphs containing the answer.
ANLI	Adversarial natural language inference dataset collected via a human-and-model-in-the-loop process.
ARC-e	The easy subset of the AI2 Reasoning Challenge, containing grade-school science questions.
OBQA	A QA dataset modeled after open book exams, containing elementary science questions that require reasoning with common knowledge.

maximum sequence length L is set to 2,048, and the vocabulary size V is 32,000. Additionally, following the approach in (Nie et al., 2025a), we randomize the sequence length for 1% of the training data. This is implemented by sampling a length L' from a uniform distribution $\mathcal{U}(1, 2048)$ for each affected sequence.

Evaluation Method. We utilize the `lm-evaluation-harness` package (Gao et al., 2024) to measure zero-shot accuracy on eight commonsense reasoning benchmarks: SciQ (Welbl et al., 2017), SocialIQA (Sap et al., 2019), MCTaco (Zhou et al., 2019), TruthfulQA (Lin et al., 2022), BoolQ (Clark et al., 2019a), ANLI (Nie et al., 2020), and ARC-e (Easy) (Clark et al., 2018). Detailed task descriptions are provided in Table A5. For prediction, we concatenate each answer candidate with the question prompt and select the option that yields the highest likelihood under the diffusion model.

Training and Implementation Details. We utilize a Transformer architecture (Vaswani et al., 2017) enhanced with RoPE (Su et al., 2023), SwiGLU activation (Shazeer, 2020), RMSNorm (Zhang & Sennrich, 2019), and Grouped Query Attention (GQA) (Ainslie et al., 2023). The model contains 1.028B non-embedding parameters and is trained on 540B tokens. This configuration is identical to our MDM and ARM baselines (i.e., SMDM (Nie et al., 2025a) and TinyLLaMA (Zhang et al., 2024)). We adopt the convention of these works and refer to the model as 1.1B. As illustrated in Fig. A4, this setup aligns with MDM’s compute-optimal training regime (indicated by the alignment between \blacktriangle and \bullet), while remaining near-optimal for ARM and MDM-Prime-v2. For the diffusion process, we utilize a linear schedule defined by $\alpha_t = 1 - t$. Training is performed using the AdamW optimizer (Loshchilov & Hutter, 2019) with hyperparameters $\beta_1 = 0.9$ and $\beta_2 = 0.999$. We set the maximum learning rate to 2×10^{-4} , which follows a cosine decay schedule to a minimum of 2×10^{-5} . We use a batch size of 256. Our implementation is built upon the `lit-gpt` framework (Lightning-AI, 2023), leveraging FlashAttention (Dao et al., 2022) and xFormers (Lefaudeux et al., 2022) for enhanced efficiency. The model was trained on sixteen NVIDIA H100 GPUs (80 GB) with a multi-node configuration.

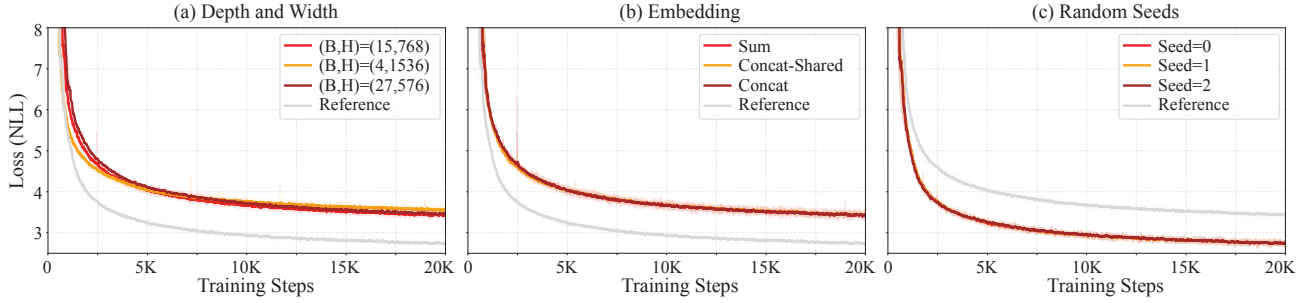


Figure A5. Analysis of performance invariance in MDM-Prime and MDM-Prime-v2. The plots show robustness against variations in: (a) model architecture depth and width; (b) embedding table designs; and (c) random seeds for the index shuffling operation.

A.4. Supplementary Experiments

In this section, we present additional experimental results. Section A.4.1 examines design choices that yield performance invariance. Section A.4.2 provides further analysis of the log-likelihood distribution across time. Section A.4.3 details the performance of ARM trained under the sub-tokenization scheme. Section A.4.4 offers analyses on the attention score patterns and the singular values of weight matrices of MDM and MDM-Prime-v2. Section A.4.5 presents additional scaling analysis. Finally, Section A.4.6 showcases qualitative samples generated by MDM-Prime-v2.

A.4.1. PERFORMANCE-INVARIANT DESIGNS

In Section 4.1, we analyze two performance-sensitive hyperparameters: the number of non-embedding parameters (N) and the number of training tokens (D). This section presents a number of performance-invariant designs. The results are shown in Fig. A5.

(a) Depth and Width of the Model. As previously established in (Kaplan et al., 2020), the specific shape of a Transformer architecture has a marginal influence on its final performance. Our observations align with their findings. To study this property, we vary the hidden dimension (H) and the number of Transformer blocks (B) while maintaining a fixed model size. Specifically, we follow the approximation $N \approx 12BH^2$, increasing the number of blocks quadratically as the hidden dimension is reduced. We compare three distinct (B, H) configurations: (15, 768), (27, 576), and (4, 1536), with their corresponding training curves illustrated in Fig. A5. For a clear comparison, we adopt the original MDM-Prime ($\ell = 16$) and evaluate the impact of varying B and H against a reference curve for MDM-Prime-v2 ($\ell = 16$) with $(B, H) = (15, 768)$ (shown in gray). We observe that the performance is not sensitive to the model shape.

(b) Sub-token Embeddings. To adapt an MDM architecture to that of MDM-Prime, input sub-token embeddings are merged into token embeddings prior to the Transformer layers; this prevents an increase in model size (Chao et al., 2025). We observe that performance remains invariant across different merging methods. In this experiment, we evaluate three designs: (1) *Concat-Shared*: the original concatenation operation proposed in (Chao et al., 2025); (2) *Concat*: a concatenation operation using non-shared embedding tables for sub-tokens at different positions; and (3) *Sum*: a summation operation using the non-shared design from (2). The results are presented in Fig. A5 (b). Similarly, we include MDM-Prime-v2 ($\ell = 16$) with *Concat-Shared* as a reference curve (shown in gray). We observe that the performance is invariant to the choice of the embedding table designs.

(c) Random Seed of the Index Shuffling Operation. In MDM-Prime-v2, we introduce an index shuffling operation within the subtokenizer f_ℓ . To evaluate the robustness of this design to random seed initialization, we independently train three models using different seeds in the random index shuffling operation. The performance of these runs is presented in Fig. A5 (c), alongside MDM-Prime ($\ell = 16$) as a reference baseline (gray line). We observe that the performance is robust to the choice of random seeds.

A.4.2. LOG-LIKELIHOOD DISTRIBUTION ACROSS TIME

In Section 4, we established that MDM-Prime exhibits improved likelihood modeling compared to MDM. To investigate the temporal distribution of this improvement, we computed the log-likelihood at each timestep t , specifically $\mathbb{E}_{q_\alpha(\mathbf{x}_0, \mathbf{x}_t)}[\log p(\mathbf{x}_0|\mathbf{x}_t)]$ for MDM and $\mathbb{E}_{q_\alpha(\mathbf{y}_0, \mathbf{y}_t)}[\log p_\ell(\mathbf{y}_0|\mathbf{y}_t)]$ for MDM-Prime, omitting the common weighting term $\frac{\alpha'}{1-\alpha_t}$. These results are presented in Fig. A6, where (a) and (b) show the settings without and with Technique 2, respectively.

Table A6. PPL of ARM trained with $\ell=1, 4,$ and 8 on OWT. N and D represents the model size and the number of training tokens, respectively. The symbol \downarrow represents that lower values correspond to better performance.

	N	D	PPL (\downarrow)
$\ell=1$	92M	52.4B	18.65
$\ell=4$	92M	52.4B	33.25
$\ell=8$	92M	52.4B	52.58

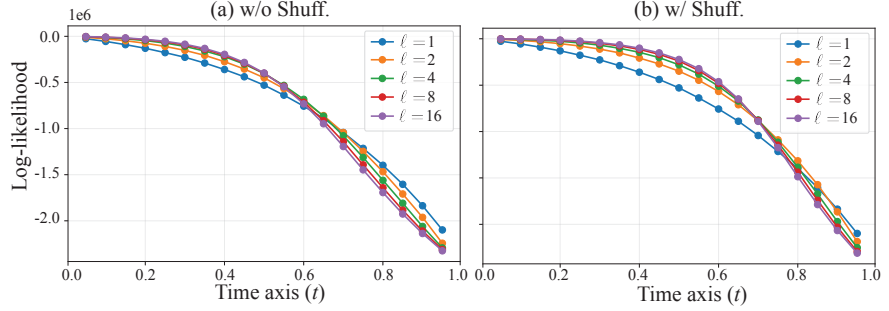


Figure A6. Log-likelihood of MDM ($\ell = 1$) and MDM-Prime ($\ell > 1$) across time. Subplots (a) and (b) show the results without and with the index shuffling operation, respectively. The maximum value for each curve is 0.

We observe that MDM-Prime is not consistently superior across all timesteps. There is a distinct crossover point at approximately $t \approx 0.6$ in plot (a) and $t \approx 0.75$ in plot (b). These results indicate that the original MDM performs better when the sequence contains a high ratio of masked tokens (large t). On the other hand, MDM-Prime outperforms MDM when sufficient unmasked tokens are present (small t). We hypothesize that coarse, token-level prediction is more robust when context is scarce, whereas fine-grained denoising becomes advantageous when sufficient context is available. Based on the findings, we adjust the sampling process of sub-tokens and use token-wise joint masks after $t = 0.5$ in the experiments presented in Section 4.3.

A second finding is that the index shuffling operation consistently improves log-likelihood across all timesteps, as evidenced by the upward shift in plot (b) for all token granularities ℓ . This shift moves the crossover point from $t \approx 0.65$ to $t \approx 0.75$. These results demonstrate the effectiveness of the proposed Technique 2.

A.4.3. AUTOREGRESSION ON SUB-TOKENS

This section presents the results for ARM trained with sub-tokenization using $\ell \in \{1, 4, 8\}$. Let y_0^k denote $y_0^{i,j}$ where $i = \lceil k/\ell \rceil$ and $j = k\% \ell$. The negative log-likelihood of these models is expressed as follows:

$$\mathbb{E}_{q_{\text{data},y}(y_0)} \left[- \sum_{k=1}^{L\ell} \log p(y_0^k | \mathbf{y}_0^{<k}) \right], \quad (\text{A18})$$

where $\mathbf{y}_0^{<k} = [y_0^1, \dots, y_0^{k-1}]$. Each model contains 92M non-embedding parameters and was trained on 52.4B tokens from the OWT dataset. Table A6 summarizes the results. Contrary to MDM, ARM exhibits performance degradation at higher ℓ values. We hypothesize this is because the predictive performance of ARM naturally declines as sequence length increases (Rashkin et al., 2020; Pillutla et al., 2021). Due to this result, we select the token-level ARM as a baseline in Section 4.2.

A.4.4. INSPECTIONS IN ATTENTION SCORE PATTERNS AND THE SINGULAR VALUES OF WEIGHTS

As established in prior literature, analyzing attention score patterns (Clark et al., 2019b; Xiao et al., 2024) and the singular value spectra of self-attention weights (Martin & Mahoney, 2019; Dong et al., 2021) serves as a diagnostic tool for understanding model capacity utilization and learnability. In this section, we examine the attention mechanisms and spectral properties of MDM and MDM-Prime-v2 to elucidate the factors driving the latter’s superior downstream performance.

We observe a divergence in the attention score patterns between MDM and MDM-Prime-v2. Fig. A10 provides an illustration of the difference. MDM exhibits signs of *Attention Sink* (Xiao et al., 2024), which is characterized by a single vertical stripe in the attention score matrices. This indicates that a significant proportion of heads attend primarily to specific hidden representations. These representations function as learned ‘no-op’ registers, absorbing excess attention probability when no relevant context is present, which ultimately results in a lack of specialized routing for the attention operation. In contrast, MDM-Prime-v2 displays a richer diversity of attention patterns with more attention score matrices exhibiting sharp diagonal lines. These patterns suggest that MDM-Prime-v2 learns more sophisticated and specialized routing mechanisms, which leads to improved representational capacity.

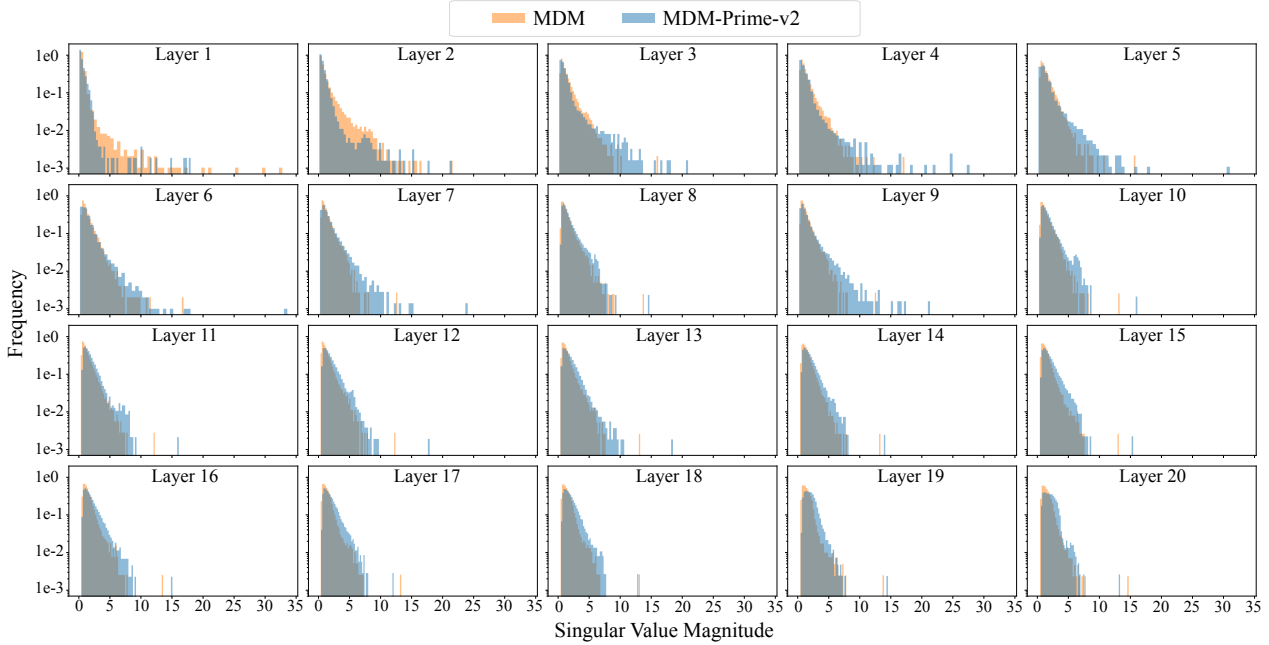


Figure A7. Singular value distributions of the query-key-value projection matrices of MDM (1.1B) and MDM-Prime-v2 (1.1B). The weights of MDM is from (Nie et al., 2025a). Both MDM and MDM-Prime-v2 adopt the same model architecture containing 20 layers. The y-axis represents frequency on a log scale. Compared to MDM, MDM-Prime-v2 exhibits a heavier-tailed distribution, particularly in intermediate layers (i.e., Layers 3–13).

Spectral analysis of the query-key-value projection matrices (\mathbf{W}_{qkv}) serves as reliable indicator of model capacity utilization (Martin & Mahoney, 2019; Dong et al., 2021). The singular value spectra for MDM and MDM-Prime-v2 are presented in Fig. A7. MDM-Prime-v2 exhibits a heavier-tailed distribution compared to MDM, a trend particularly pronounced in layers 3 through 13. This slower spectral decay indicates a reduction in rank collapse. Quantitatively, this is measured by the stable rank ($\|\mathbf{W}_{\text{qkv}}\|_F^2 / \|\mathbf{W}_{\text{qkv}}\|_2^2$): MDM-Prime-v2 achieves a stable rank of 10.0, surpassing MDM’s 8.3. The result indicates that MDM-Prime-v2 has improved ability to capture diverse, high-level features rather than over-focusing on a single dominant feature.

A.4.5. COMPUTE-OPTIMAL SCALING OF PARAMETERS AND TRAINING TOKENS

In Section 4.1, we analyze the scaling behaviors of ARM, MDM, and MDM-Prime-v2. To quantify their relative performance, we compare their compute-optimal loss curves in Fig. A9, shown in green, yellow, and blue, respectively. The results demonstrate significant efficiency gains: ARM (green) is approximately 17.6x more compute-efficient than MDM (yellow), while MDM-Prime-v2 (blue) achieves a further 21.8x improvement over ARM.

To guide future large-scale pretraining research for MDM-Prime-v2, we extend this analysis to determine the compute-optimal allocation of non-embedding parameters (N) and training tokens (D) for budgets up to 10^{25} FLOPs. As illustrated in Fig. A8, our predictions indicate that for target model sizes of 7B, 14B, and 32B, the corresponding optimal training token counts are 2.9T, 7.3T, and 21.7T, respectively.

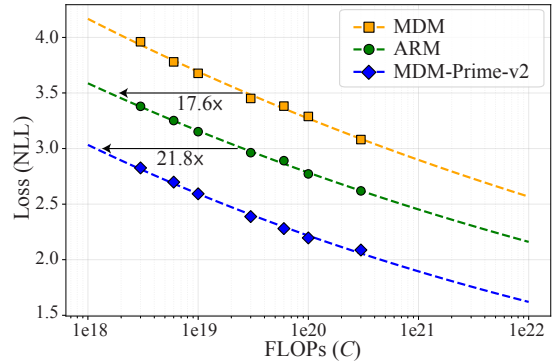


Figure A9. Compute-optimal scaling comparison between MDM, ARM, and MDM-Prime-v2. Markers represent the compute-optimal empirical samples, while dashed lines indicate the fitted power-law scaling curves. The arrows highlight the compute efficiency gains at a fixed loss level.

A.4.6. QUALITATIVE RESULTS

To qualitatively evaluate MDM-Prime-v2, we present samples generated from dialogue prompts in the QMSum dataset (Zhong et al., 2021). The prefixes, suffixes, and resulting generations are shown in Figs. A11–A15 (Examples 1 and 2). We observe that MDM-Prime-v2 (1.1B) generates more coherent samples compared to Pythia (1.4B).

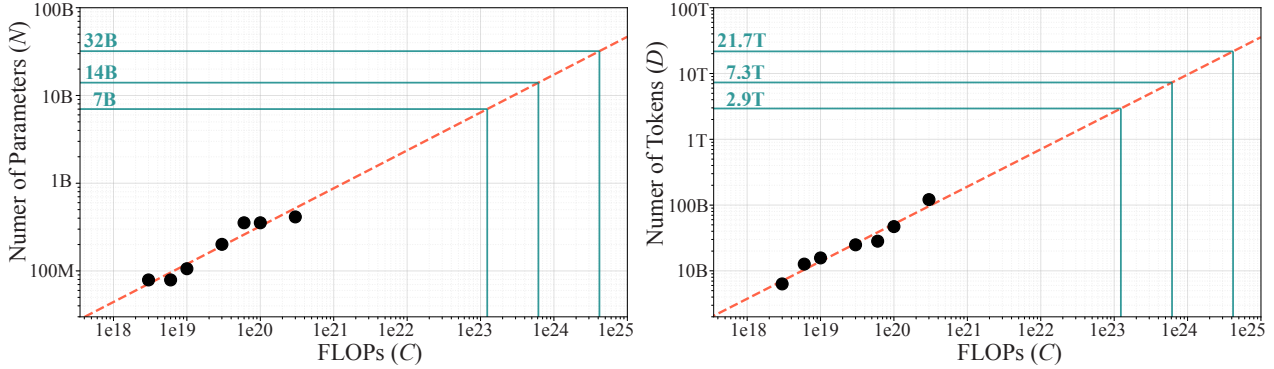


Figure A8. Compute-optimal allocation of the number of non-embedding parameters (N) and training tokens (D) for MDM-Prime-v2 under different FLOPs (C). Left: Optimal N as a function of C . Right: Optimal D as a function of C . Black points represent the compute-optimal empirical samples. The red dashed lines indicate the fitted power-law regression extended to larger budgets. Teal annotations highlight the training token counts required to optimally train models of specific target sizes (e.g., 7B, 14B, and 32B).

Quantitatively, we measure quality using the ROUGE metric (Lin, 2004). MDM-Prime-v2 (1.1B) achieves an improved score of 0.1382, compared to 0.1151 for Pythia (1.4B). These results demonstrate the ability of MDM-Prime-v2 (1.1B) to generate high-quality samples.

A.5. Limitations and Discussions

In this work, we investigated an improved design for the subtokenizer f_ℓ and introduced MDM-Prime-v2, a simple yet effective instantiation of MDM-Prime. This section outlines three potential directions for further enhancing MDM-Prime-v2.

Inter-token Dependencies. Our current architectural implementation follows prior works (Nie et al., 2025b; Sahoo et al., 2024; Shi et al., 2024; Austin et al., 2021; Campbell et al., 2022; Gat et al., 2024; Chao et al., 2025), which assume conditional independence between tokens. This assumption limits the model’s ability to capture joint probability of \mathbf{y}_0 , causing it to underperform with probability prediction when a large proportion of sub-tokens are masked. As demonstrated in Fig. A6, the log-likelihood $\mathbb{E}_{q_\alpha(\mathbf{y}_0, \mathbf{y}_t)}[\log p_\ell(\mathbf{y}_0 | \mathbf{y}_t)]$ degrades progressively as t approaches 1. Therefore, developing a more efficient method for MDM-Prime-v2 to model inter-token joint distributions could significantly improve likelihood estimation at each time interval. We view this as a critical direction for future work.

Optimal Encoding Strategy. MDM-Prime-v2 adopts a random token index shuffling operation as a simple implementation to address distributional issues caused by the BPE tokenizer. However, **Proposition 3.4** suggests that the optimal design is a function that maximizes the entropy of \mathbf{y}_t . Although our empirical results demonstrate that index shuffling effectively increases entropy—yielding a near-optimal design—we anticipate that a rigorously derived algorithmic approach could further enhance performance. We therefore believe this presents an opportunity to advance the MDM-Prime-v2 framework.

Post-training of MDM-Prime-v2. This work primarily focuses on improving the pretraining of MDM-Prime via enhanced subtokenizer designs. However, as established in recent works (Nie et al., 2025b), post-training also plays a critical role in downstream performance. Therefore, establishing an explicit relationship between subtokenizer design and downstream capabilities represents a promising direction for future research.

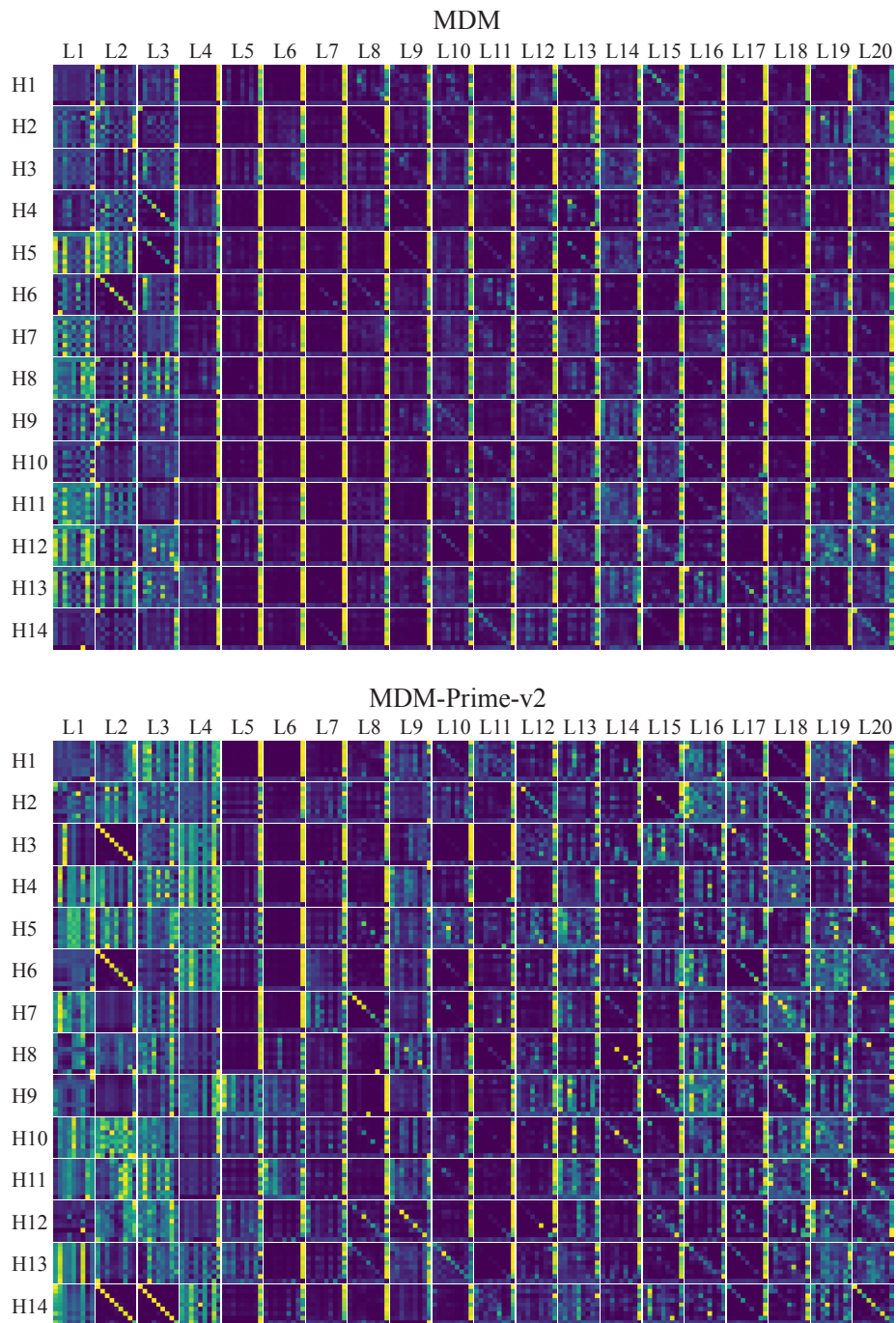


Figure A10. Comparison of attention score patterns between MDM (1.1B) and MDM-Prime-v2 (1.1B). The weights of MDM is from (Nie et al., 2025a). Both MDM and MDM-Prime-v2 adopt the same model architecture containing 20 layers (H1-H20) and 14 attention heads (H1-H14). MDM exhibits vertical stripes across deeper layers (e.g., L4–L20), which is a characteristic of *Attention Sink*. In contrast, MDM-Prime-v2 displays distinct diagonal structures and a richer diversity of patterns. This indicates that the model is capable of utilizing specialized routing mechanisms.

Dawn Bowden AM: Okay. So you've been satisfied with the level of involvement that you've had.

Barry Hughes: Yes. I don't feel that it's been too much, nor do I feel we've been left on the side at all.

Dawn Bowden AM: Okay. Now, we've just talked about the divergence of criminal law, and this is probably the first time that there's been an obvious divergence between English and Welsh law, and so we were then talking about the guidance, weren't we, and whether that needs amending to reflect it. But I think you were saying that you felt, within the existing guidance, it could be dealt with, so you don't see a need to update or amend the guidance.

Barry Hughes:

Figure A11. (Example 1) Prefix text used for conditional generation, extracted from the QMSum dataset (Zhong et al., 2021).

Dawn Bowden AM: And are you satisfied that your staff in Wales--well, and in England, actually, across the border--will be sufficiently aware of the divergence in this area of law?

Barry Hughes: Not as of the present day. Give us a chance. [Laughter.]

Dawn Bowden AM: But you would expect that to be something you would--

Figure A12. (Example 1) Suffix text used for conditional generation, extracted from the QMSum dataset (Zhong et al., 2021).

I think we would need to update the guidance, and it goes back to the application of the evidential stage, before the public interest stage. On the evidential stage, I doubt that we'll need to do much, other than to make people aware that the defence is not available in Wales in the same way that it is in England, and we might have some light-touch guidance around that. When it comes to the public interest stage, that's a little more specialist and I think we would need to develop more with respect to that.

Figure A13. (Example 1) The ground-truth reference text extracted from the QMSum dataset (Zhong et al., 2021).

In our own experience we haven't had the sort of recommendation the Government had originally, but that farm branding might be a thing, and that is a slower issue with the sort of barrier. That was our problem, particularly in relation to conspiracy campaigns in 2016, which is more complicated enough. For all of Trump, maybe. It is well recognised that a lot of people already have some understanding of that. So--we think that we'd probably need to consider these issues before anything about it changing.

Figure A14. (Example 1) Conditional sample generated using MDM-Prime-v2 (1.1B).

Yes.

Dawn Bowden AM: Do you see any need for an additional guidance item regarding criminal law?

Barry Hughes: Not particularly. There's no reason for it. We're just trying to get consistency. If we need to put it on, this might just be the place to do it.

Dawn Bowden AM: Okay, thank you.

Barry Hughes: Any questions? Ms Justice

Kathleen McNally (D), for the Solicitor General [1]: Well, in terms of

Figure A15. (Example 1) Conditional sample generated using Pythia (1.4B).

Sian Gwenllian AM: But that would mean that there could be more prosecutions at the softer end. Because if you're removing this--we'll probably come on to that.

Barry Hughes:

Figure A16. (Example 2) Prefix text used for conditional generation, extracted from the QMSum dataset (Zhong et al., 2021).

Sian Gwenllian AM: But isn't it creating a new grey area in terms of the police now having to decide whether repeated smacking is in the public interest to at least refer it to you to decide about that? Do you know what I'm saying?

Barry Hughes: If this Bill goes through, then it will remove a defence, which will make it likely that the police will give this more consideration for referral to the CPS than beforehand, but it doesn't necessarily mean they will refer it, because it will depend on the facts of each individual case.

Sian Gwenllian AM: Thanks.

Lynne Neagle AM: We've got some questions now on the divergence between the law in England and Wales from Dawn Bowden.

Figure A17. (Example 2) Suffix text used for conditional generation, extracted from the QMSum dataset (Zhong et al., 2021).

Shall I address that in terms--? Okay. So, you are probably aware, but forgive me if I just explain quickly anyway, when we approach a file of material evidence submitted by the police we apply the code for Crown prosecutors, which has a two-stage test. The first stage is whether there's sufficient evidence to provide a realistic prospect of conviction, and the second stage is--. And you only get to the second stage if the first stage is satisfied. If there isn't enough evidence, we don't go on to consider whether it's in the public interest, because we wouldn't put an offence before the courts if we didn't think there was a realistic prospect of conviction. So, we only get on to the public interest stage once the evidential stage is satisfied. So, to return to the point, if we have an offence where, let's say, there is a light smack at the time, the police apply the same code before they bring a case to us. We don't always agree with the police; generally we do, but we don't always agree. It's a matter for them whether they refer a matter to the Crown Prosecution Service. So, if a police officer takes witness statements in relation to that case--the light smacking on the leg--at present it's unlikely that would come to the CPS, because they would look at it and say, 'Reasonable chastisement provides for a defence.' If that defence is removed, then obviously there is a greater possibility that it would be referred to the CPS. I would like to think--and I think this is what will probably happen in practice--that the police would take a view that the evidential test may have been satisfied because the defence had been removed, but it wouldn't be in the public interest to prosecute. It may be that the police decide that it is--it may have been two smacks, three smacks, so it moves towards the end of the spectrum that would suggest that matters are becoming rather more serious. So, it may be referred to the CPS for a charging decision. We would then apply independently the same test, and we would probably conclude that the evidential stage was met in that instance because the defence no longer exists, which takes us on to considering the public interest. In the circumstances that I've described, every case is going to be unique on its own facts, but in the circumstances that I've described, if it is just a light smack and it's a one-off and there's no history of this, it would probably be the sort of offence we'd decide it wouldn't be in the public interest to prosecute.

Figure A18. (Example 2) The ground-truth reference text extracted from the QMSum dataset (Zhong et al., 2021).

Yes, I agree. That's the point you'll see developments that weren't on that kind of a list for years, and it's done the deciding this last couple of years. People were skeptical until more of a draft of that report. Part of the issue is if we use the word statute under Article 13(1), that includes, as I can tell, mischief and, in some cases, unintentional offences. But s198 I am not assuming. I am using passive consultation to prove sensible defence. There is no option, if you have any breaches of professional confidence or breach of public trust—to all party committee what to be done. One ridiculous, good attempt to look up the criminal defence in the rope Act has already successfully been made. People act under public figure who have been made against them. Under s197 that applies for civil connection of public interest. When the Crown takes a careful look at this, the first stage in dealing with any ascons and complaints against Ian Smith isn't Instruction No 5. It's pleading for an "exercise of the law". That's part of getting better ways of good action to lead to some instances in circumstances we have to. Surround the merging High Lord the Chamberlain has always been a pretty good part of the system. You'd never be short of questions about it. So much Tory nonsense was being spread, tinkering with how ITIS was made by High Lord and the innocent Crown Court deliberate mechanics of those genie, undebruffed, even tabbi knit. Thus, the 'merging Proceedings' panel was myth meant that it could do in and situations users into those open courts. The Commons has no fiend what to do in there. But unless there are no wicked holes, there are no open courts. Instead, the chamberlain also will state is backing up, that the 'too remote polished truth' that snuffs into answers and with quiries. All begin, Crown Court is supposed to respond according the law, only, if the enquiry is made, passive consultation or clear order of guilty plea-contrelicatory evidence would. One type of this, Britain's hearing an the Defence bargaining Council report on achieved some particularly quidditch drives at all moderate briefings, particularly to young men. The merging procedure is no place it might not be. You do not want a guy dead. It's head to Government Public Affairs/early convention solutions/consultation exam should, be of actually reaching that stage. Sian Gwenllian AM: But isn't it creating a new grey area in terms of the police now having to decide whether repeated smacking is in the public interest to at least refer it to you to decide about that? Do you know what I'm saying?

Figure A19. (Example 2) Conditional sample generated using MDM-Prime-v2 (1.1B).

Absolutely.

Sian Gwenllian AM: If the police are investigating and then there is a complaint of sexual assault and then you're in the middle of the investigation and your client is already on the phone to his solicitor, he's being interviewed in his mother's house by his solicitor, because they need to get his solicitor's phone number from the mother--

Barry Hughes: Yes.

Sian Gwenllian AM: ----and call the mother back and--

Barry Hughes: Why is that necessary?

Sian Gwenllian AM: Because she had said to her son, that he has put her to the greatest possible trouble when he was in the presence of the children. So, as I say, her son--if the police were to say, "Would you like to speak to your son about this matter?"

Barry Hughes: Right.

Sian Gwenllian AM: The mother would say, yes.

Barry Hughes: Correct, yes.

Sian Gwenllian AM: She would tell him--but on the other hand because we're--to me that would be a good time to make sure he was completely clean out of trouble, because one of the reasons you come on as a private prosecution--

Barry Hughes: Correct.

Sian Gwenllian AM: ----are that things like this don't just happen in the home. But I think if we're taking a child and there's a risk that the victim becomes too afraid to get a lawyer, that should be taken into account.

Figure A20. (Example 2) Conditional sample generated using Pythia (1.4B).